Photoacoustics 28 (2022) 100426

Contents lists available at ScienceDirect

Photoacoustics

journal homepage: www.elsevier.com/locate/pacs

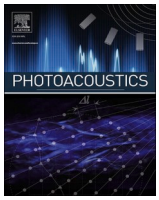

Design and application of organic contrast agents for molecular imaging in the second near infrared (NIR-II) window

Zhen Jiang [a,1], Yuanmeng Ding [a,1], Jonathan F. Lovell [b], Yumiao Zhang [a,*]

[a] School of Chemical Engineering and Technology, Key Laboratory of Systems Bioengineering (Ministry of Education), Frontiers Science Center for Synthetic Biology (Ministry of Education), Tianjin University, 300350, China
[b] Department of Biomedical Engineering, State University of New York at Buffalo, Buffalo, NY 14260, USA

ARTICLE INFO

Keywords:
Second near infrared (NIR-II)
Organic dyes
Imaging contrast agents
Photoacoustic imaging
Fluorescence imaging

ABSTRACT

Optical imaging in the second near-infrared (NIR-II) window has attracted interest in recent years because of the merits of reduced light scattering, minimal autofluorescence from biological tissues and deeper penetration depth in this wavelength range. In this review, we summarize NIR-II organic contrast agents reported in the past decade for photoacoustic and fluorescence imaging including members of the cyanine family, D-A-D structure dyes, phthalocyanines and semiconducting polymers. Improved imaging contrast and higher resolution could be favorably achieved by rational design of NIR-II fluorophores by tuning their properties including molar extinction coefficient, fluorescence quantum yield, emission wavelength and others. A wide variety of applications using NIR-II dyes has been realized including imaging of tumors, lymphatics, brains, intestines and others. Emerging applications such as targeted imaging and activable imaging with improved resolution and sensitivity have been demonstrated by innovative chemical modification of NIR-II dyes. Looking forward, rational design of improved NIR-II dyes for advanced bioimaging is likely to remain an area of interest for next-generation potential approaches to disease diagnosis.

1. Introduction

Various biomedical imaging techniques provide tools for disease diagnosis and therapeutic management in clinics [1,2]. Over the past decades, the development of a number of imaging modalities has been the focus of considerable research, such as fluorescence imaging, photoacoustic imaging, positron emission tomography (PET), magnetic resonance imaging (MRI) and others. Optical imaging has advanced rapidly preclinically and holds promise in the clinic owing to the advantages of nonionizing radiation and high spatiotemporal resolution [3,4]. Advantages are more pronounced in the near-infrared window (NIR), where background is lower and tissue penetration is greater. Compared to the first near-infrared (NIR-I; 700–900 nm) window, the second near-infrared (NIR-II; 1000–1700 nm) window can achieve higher signal-to-noise ratio (SBR) and deeper tissue penetration resulting from lower tissue autofluorescence and lower signal attenuation [5–8]. As such, current optical imaging approaches including FL imaging, PA imaging, self-luminescence [9,10] are being investigated in the NIR-II window for imaging of tumors [11–14], lymph nodes and lymphatic vessels [15–18], specific organs (such as intestines and ovarian) [19,20] and disease microenvironment [21–25]. In addition, NIR-II imaging has potential for imaging in deeper biological tissues in a noninvasive manner to obtain detailed and accurate information [26,27]. Altogether, the development of NIR-II contrast agents has attracted a great deal of recent research efforts [28–30].

Broadly, NIR-II contrast agents can be divided into inorganic and organic ones. Inorganic NIR-II contrast agents including single-walled carbon nanotubes [31–33], quantum dots [34–36], rare earth compounds [37–39], metal-based compounds [40–42], noble metals [43–45] can exhibit strong optical absorbance, high brightness and resolution, and can even be active in the NIR-IIa window (1300–1500 nm, smaller optical sub-windows). However, the long-term toxicity is arguably a potentially dauting concern for their translation to humans. In contrast, organic NIR-II contrast agents are considered to have better biocompatibility, clearance and biodegradability. Safety is crucially important for clincal translation of NIR-II molecules and related nanoparticles. Ideal optical contrast materials should be easily metabolized and cleared by hepatobiliary or renal clearance pathways. It was shown

* Corresponding author.
E-mail address: ymzhang88@tju.edu.cn (Y. Zhang).
[1] These authors contributed equally to this work and should be considered co-first authors.

https://doi.org/10.1016/j.pacs.2022.100426
Received 10 August 2022; Received in revised form 5 October 2022; Accepted 14 November 2022
Available online 15 November 2022

that semiconducting polymer nanoparticles could be enzymatically degraded by the mononuclear phagocyte system (MPS) and myeloperoxidase (MPO), followed by elimination through hepatobiliary and/or renal excretion [46]. Particularly, renal-clearable optical agents (RCOAs) minimize the side effects for bioimaging since they could be rapidly filtered by the glomerular filtration membrane, subsequently transported via renal tubules and then execreted by urine. Size, charge, and chemical composition, shape and others are determination factors for the clearance pathways [47].

In addition, the physical and chemical properties of NIR-II dyes can be tuned by rational design, including molar extinction coefficient, fluorescence quantum yield, emission wavelength and others [28, 48–50]. Many strategies for improving these parameters could be employed. For example, in order to achieve deeper penetration depth, endeavors could be made by tuning the intramolecular charge transfer for bathochromic shift. Moreover, highest occupied molecular orbital (HOMO), lowest unoccupied molecular orbital (LUMO), band gap level, donor and acceptor selection and the electronegativity of the donor and acceptor groups are also some important considerations for rational design of NIR-II contrast agents.

Most organic NIR-II contrast agents are intrinsically hydrophobic; thus commonly used methods of improving water solubility include: covalently conjugation to hydrophilic moieties (e.g. polyethylene glycol (PEG)) [51–53], encapsulation in an amphipathic carriers (e.g. DPPC, DSPE-mPEG2000) [54–56] and entrapment by surfactants or polymeric nanoparticles (e.g. Pluronic F127, Tween, PEG-b-PPG-b-PEG) [57–59]. Fluorescence (FL) imaging and photoacoustic (PA) imaging are two important optical imaging modalities. A plethora of contrast agents with fluorescence emission or absorption in the NIR-II region have been designed [5]. Although it might difficult to reconcile multiple imaging modalities and improving one possibly compromises another, there still exist some exquisitely designed contrast agents for multimodal imaging such as both NIR-II FL and PA imaging [16,60]. Meanwhile, more principles and examples of NIR molecular design was recently illustrated by Mu et al. [61]. The chemical modification and self-assembly of NIR-II probes can also enhance multimodal imaging, providing more accurate and enriching information [62–64]. In addition, design of “smart” multifunctional organic NIR-II contrast agents has been demonstrated. Targeted organic NIR-II probes show higher accumulation in specific biological sites with reduced background noise and amplified imaging signal [65–67]. Activatable NIR-II probes could be “turned on” in response to specific pathological conditions, such as hypoxia, low pH, reactive oxygen species and small molecule mediators in tumors. As a result, qualitative analysis with higher signal-to-background ratio can be achieved [68,69].

In this review, we overview recently reported organic dyes in the NIR-II window and their applications for bioimaging. First, the designs, structures and categories of NIR-II dyes are summarized with an emphasis on probes demonstrated for use in fluorescent and photoacoustic imaging. Then, we overview some of their applications for fluorescence imaging, photoacoustic imaging and multimodal imaging. Also, the chemical modification of dyes for the synthesis of smart probes for functional imaging (targeting imaging and activatable imaging) is also discussed.

2. Design, structure and categories of NIR-II dyes

In this section, we primarily focus on NIR-II dyes for the applications of photoacoustic imaging and fluorescence imaging. The biophysical mechanisms of these imaging are shown in the simplified Jablonski diagram in Fig. 1. Briefly, once the chromophore is excited upon illumination, electrons in photosensitizers transit from the ground state to an excited singlet state. Excited molecules tend to return to the grand state in different pathways including radiative and non-radiative decay. The former provides the basis for fluorescence imaging. The photon emission or quenching comes with heat generation and heat dissipation is the basis for photothermal therapies. Non-radiative decay enables photoacoustic imaging, photodynamic therapy, photothermal therapy and photothermal imaging. The photoacoustic effect is based on the absorption of photons by biological molecules thermoelastically, which generates high pressure around the contrast agents and ultrasonic wave. Therefore, the photoacoustic signal intensity is directly related to the molar extinction coefficient of contrast dye [70]. However, some of these processes are competitive to each other. For example, if a probe has high fluorescence efficiency, the PA signal generated from it would be low since input optical energy is dissipated via fluorescence instead of heat. Therefore, rational design of organic fluorophores could provide solutions to reconcile this challenge. For example, NIR-II AIEgen allowing fluorescence imaging, photoacoustic imaging, photothermal imaging, photodynamic imaging and photothermal therapy was developed by controlling molecular motions to strike the balance between radiative and nonradiative decays [71].

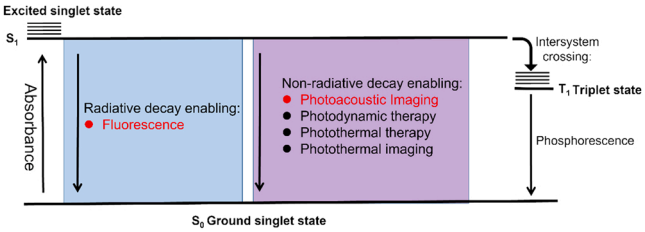

Fig. 1. Simplified Jablonski diagram illustrating some excited state decay pathways after chromophore activation.

2.1. NIR-II fluorescent probes

To extend the emission wavelength of organic NIR-II fluorophore to NIR-II region, the strategies of rational design of molecular structures include increasing the length of the conjugate chain, reducing the energy gap between the HOMO and LUMO, and selecting reasonable molecular backbones and substitutional groups. Moreover, the high quantum yield (QY) and large absorption coefficient are also relevant to the performance of NIR-II fluorophores. Broadly, many NIR-II fluorescence probes can be categorized into cyanine dyes, dyes with donor-acceptor-donor (D-A-D) structure, conjugated polymers, modified NIR-I dyes and others. Among these, cyanine dyes and D-A-D structure dyes are the most common and representative, and have been extensively used in preclinical studies.

2.1.1. Cyanine dyes

Cyanine dyes in the NIR-I have been used for decades and many in the NIR-II windows have also been developed. Indocyanine green (ICG), is a United States Food and Drug Administration (FDA) clinically approved fluorescent contrast agent in the NIR-I region, and is thus an important example of a cyanine dye. The safety and biocompatibility of ICG has been demonstrated in human studies [72]. Cyanine dyes are typically composed of two indolenine groups connected by different amounts of vinyl bonds. The vinyl bonds or bilateral indolenine groups can be chemically modified to improve their chemical and optical properties [28]. The substitution of a rigid cyclohexene in the center of the vinyl bonds significantly enhances the photostability and QY [73]. Bilateral substitutional groups can be conjugated including the ionic groups at the end of conjugated chain, such as sulphonic groups for redshift emission or better water solubility. A myriad of cyanine dyes is commercially available. Fig. 2 shows several representative chemical structures of cyanine dyes in NIR-I or NIR-II regions.

Similar to the spectrum of ICG, IR-820 exhibits both absorption and emission peaks in the NIR-I region, but its emission tail (detected by InGaAs spectrometers) extends to the NIR-II region (Fig. 3a) [17]. Similar optical properties also applies for IR-783 [74], IRDye800CW [75], IR-12N3 [76] etc. Feng et al. found a bathochromic shift for the

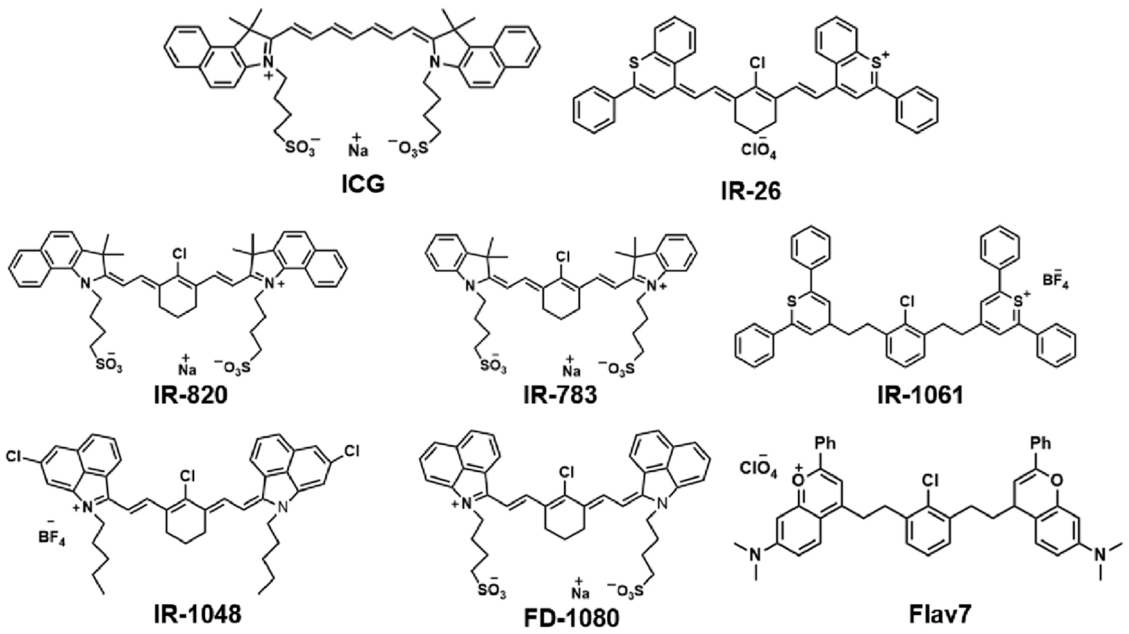

Fig. 2. Typical chemical structures of cyanine dyes in NIR-I/II windows including ICG, IR-820, IR-783 (emission tail at 1000–1400 nm), IR-26 (emission at 1082 nm), IR-1061 (emission at 1064 nm), IR-1048 (emission at 1046 nm), FD-1080 (emission at 1080 nm), Flav7 (emission at 1045 nm).

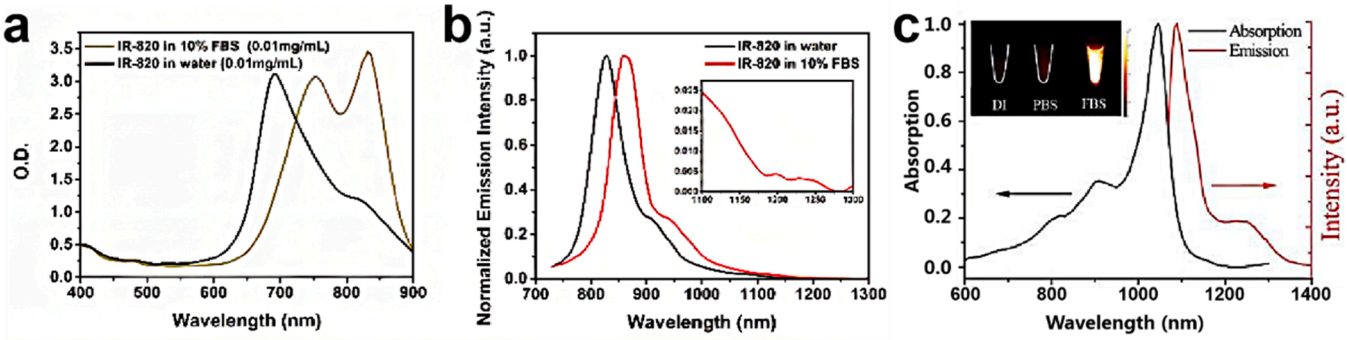

Fig. 3. Optical properties of representative cyanine dyes a) Absorption spectra and b) Fluorescence emission spectra of IR-820 (0.01 mg/mL) in water and 10% FBS. Inset: emission spectral window beyond 1100 nm [17]. c) Absorbance and fluorescent emission spectrum (1064 nm laser excitation) of FD-1080. Inset: NIR-II fluorescence image of FD-1080 in deionized water, FBS, and PBS [78]. KGaA, Weinheim, Copyright 2018.
(a) A-b) Reproduced from ref. (b) C) Reproduced from ref. (c) 17 with permission from the Ivyspring International Publisher, Copyright 2019. (d) [78] with permission from Wiley-VCH Verlag GmbH & Co.

whole spectral region when IR-820 was dissolved in 10% fetal bovine serum (FBS) compared to that in water, probably because serum proteins were absorbed on IR820 molecules, which was also verified by size measurement by dynamic light scattering. And the emission tail even extended to over 1000 nm (Fig. 3b). The NIR-II fluorescence intensity ratio was calculated to be up to 30%, and the NIR-II QY increases from 0.313% to 2.521% (IR-26 as a reference) [17].

Unlike the aforementioned fluorophores, IR-1061 exhibits an absorption peak in the NIR-I window and an emission peak in the NIR-II window, therefore, it can be employed as both NIR-I PA contrast agent and NIR-II FL contrast agent [65]. Similar fluorophores also includes IR-1048 and others [77]. Li et al. designed and synthesized a fluorophore termed FD-1080 with maximal absorption and emission wavelengths in 1064 nm and 1080 nm, respectively (Fig. 3c). Similarly, the QY of FD-1080 significantly increased from 0.31% to 5.94% (ICG as a reference) after mixing in fetal bovine serum (FBS). Besides, FD-1080 also showed outstanding aqueous solubility, high biocompatibility and photostability [78]. Flav7 was also shown to have similar optical properties [53]. BIBDAH is a comercially avaiable NIR-II cyanine dye that can be easily formulated for contrast imaging [79].

2.1.2. *D-A-D structure dyes*

Donor-Acceptor-donor (D-A-D) structures, based on benzobisthiadiazole (BBTD) as a central acceptor, have been extensively studied for the development of NIR-II probes [80]. BBTD is heterocyclic quinoid features a strong electron withdrawing group, combined with electron donating groups via aromatic π-bridging linkers on either side. The intramolecular charge transfer to reduce energy gaps result in NIR-II emission [81]. Since the first-generation D-A-D structural NIR-II fluorophore named CH1055 based on BBTD was reported by Antaris and co-workers, this type of dye has attracted significant research interest. Fig. 4 summaries some reported NIR-II fluorophores with a D-A-D structure. CH1055 adopted triphenylamine as donor and then four carboxylic acid groups were introduced in triphenylamine to provide water solubility and allow further modification such as conjugation with targeting ligands. The excitation and emission peaks of CH1055 are about 750 nm and 1055 nm, respectively. The emission tail is within the NIR-IIa region. The QY of CH1055 is about 0.3%, using IR-26 as a reference. Furthermore, CH1055 also exhibits fast excretion (about 90% excreted through the kidney within a day) and good photostability [82]. Subsequently, a variety of electron donating units, π-bridging linkers

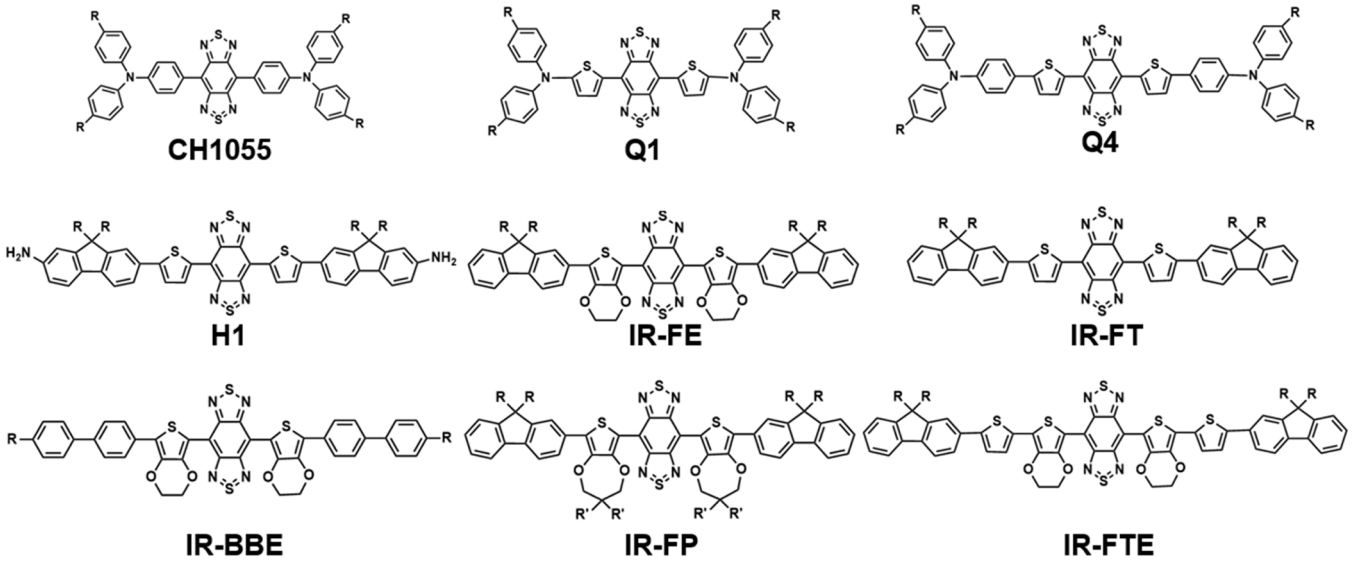

Fig. 4. Chemical structure of D-A-D/S-D-A-D-S fluorophores based on BBTD core.

and terminal functional groups could be designed and tuned to optimize fluorophores [48]. A series of CH1055 derivatives were also designed and synthesized. Sun et al. reported four kinds of fluorescent compounds (Q1, Q2, Q3, and Q4) and investigated the relationship between their structures and optical properties. Among them, Q1, Q4 displayed emission in the NIR-II region and Q4 was considered the most promising NIR-II fluorophore because of better fluorescence properties [83]. Specifically, Q1-Q4 were made by incorporating a thiophone spacer based on the D-A-D scaffold. Q2 and Q3 both selected 4,7-dibromo-5, 6-dinitro-2,1,3-benzothiadiazole as the acceptor but displayed NIR-I emission, which are not suitable for future investigation of NIR-II imaging. Q1 and Q4 share the same acceptor structure (benzobisthiadiazole, BBTD) but with different side chains. The NIR-II emission of Q4 was shown to be longer than Q1 because of formation of a strong charge transfer structure between their D–A–D units. Then, Sun et al. proposed another deliberately designed NIR-II dye termed H1 (with 2-amino 9, 9-dialkyl-substituteduorene as both donor and protecting groups) with fluorescence emission around 1100 nm in the NIR-II region (Fig. 5a) and with fluorescent brightness better than Q4 (Fig. 5b) [84].

D-A-D structured fluorophores may suffer from some disadvantages

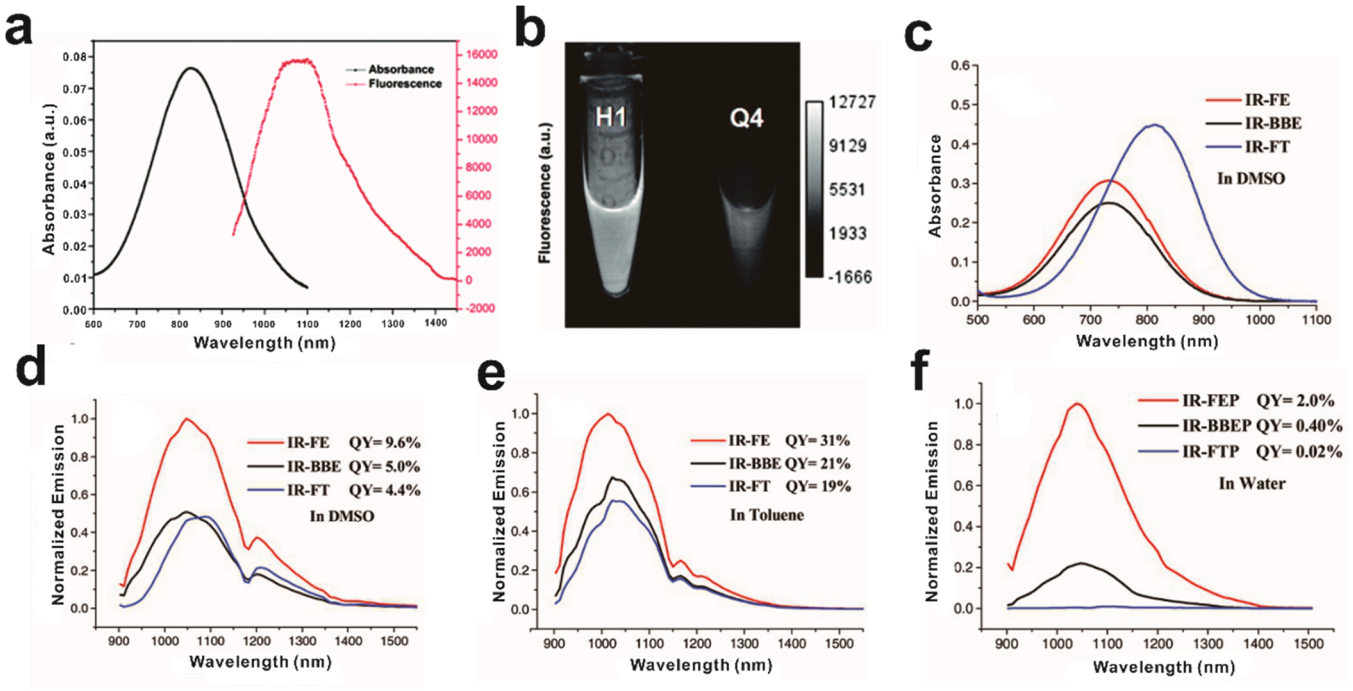

Fig. 5. Spectral characteristics of representative NIR-II fluorescence dyes. a) Absorbance and fluorescence emission spectra (808 nm laser excitation) of H1 (10 ms exposure time). b) Comparison of NIR-II fluorescence signals of H1 and Q4 (808 nm laser excitation, 20 ms exposure time) [84]. c) Absorption and d) Fluorescence emission spectra of IR-FE, IR-BBE, and IR-FT in DMSO; e) Fluorescence emission spectra of IR-FE, IR-BBE, and IR-FT in toluene. f) Fluorescence emission spectra of IR-FEP, IR-BBEP, and IR-FTP in water (imaging detail: 808 nm laser excitation, 50 ms exposure time) [85]. KGaA, Weinheim, Copyright 2017.
(a) A-b) Reproduced from ref. (b) C-f) Reproduced from ref. (c) [84] with permission from the Royal Society of Chemistry, Copyright 2017. (d) [85] with permission from WILEY-VCH Verlag GmbH & Co.

such as poor long-term stability, fluorescence quenching, which limits their development and applications. To solve these problems, the introduction of shielding (S) moieties at the end of the fluorophores, giving rise to an S-D-A-D-S structure, could effectively protect the core structure of fluorophores from fluorescence-quenching caused by intermolecular interactions and molecular-water interactions. Base on the S-D-A-D-S structure with BBTD as central acceptor, many common donor units can be used for the rational design of fluorescent fluorophores including thiophene, triphenylamine, 3, 4-ethylenedioxy thiophene (EDOT), 3, 4-propylenedioxy thiophene(PDOT) and their derivatives. Shielding groups usual contain dialkyl substituted fluorene, benzene, diphenylamine, triphenylamine and their derivatives.

Some endeavors have also focused on the development of different fluorophores with an emphasis of comparative studies. Yang et al. constructed three molecular fluorophores named IR-FE, IR-FT, IR-BBE with BBTD-based S-D-A-D-S structure. PEG chains were introduced to the terminals of the fluorophores by click chemistry to form water-soluble fluorophore counterparts named IR-FEP, IR-FTP, IR-BBEP. Then they systematically evaluated the physical properties, geometric, electronic and optical properties via density functional theory (DFT) and time-dependent DFT (TDDFT). Despite the different absorption peaks of the three compounds, they exhibited similar emission peaks around 1047 nm (Fig. 5c-f). Furthermore, compared to IR-FT with thiophene as the donor units, IR-FE with 3, 4-ethylenedioxy thiophene (EDOT) as the donor can achieve larger backbone distortion, lower delocalized LUMO and better electrostatic potential distribution. And compared with the shielding counterpart in IR-BBE, dialkyl substituted fluorene can preferably protect the BBTD backbone from aggregation-induced fluorescence-quenching due to the molecular-water interaction and intermolecular interactions. Owing to EDOT and fluorene, the fluorescence QY of IR-FE and IR-FEP reached 31% (in toluene) and 2% in aqueous solution, respectively, which are superior results compared to others (Fig. 5e, f) [85]. Subsequently, Yang et al. also demonstrated that the introduction of thiophene as the second donor could further extend the conjugated chains, resulting in a bathochromic shift of fluorescence [86].

2.1.3. Others

Besides cyanine and D-A-D type of dyes, other NIR-II fluorophore types include DD-A-DD, A-D-A, A-A [87–90]. Conjugated polymers formed by polymerized electron-rich donor monomers together with electron-deficient acceptor monomers could lead to red shifting to the NIR-II region by intermolecular electron transfer effect between the donor and acceptor units. Lu et al. successfully synthesized a novel polymer conjugate named DPP-TT, which consists of diketopyrrolopyrrole (DPP) as an electron withdrawing unit and fluorothieno-[3, 4-b] thiophene (TT) as an electron donating unit. After encapsulating DPP-TT into DSPE-mPEG5000 matrix, the resulting DPP-TT exhibited strong emission in the NIR-II window [91]. The selection of appropriate electron withdrawing units and electron donating units is also important for the construction of conjugated polymers with desirable optical properties. Careful design of conjugated polymers not only induced fluorescence properties in the NIR-II window but also strong absorption and photoacoustic characteristics [91–93].

Other NIR-II fluorophores can be obtained by engineering existing dyes such as squaraine, porphyrins, xathenes, or pathalocyanine. Yao et al. developed NIR-II squaraine dye named SQ1 by engineering the D-A-D structured squaraine dye with saquric acid as the electron acceptor and ethyl-grafted 1, 8-naphtholactam as the electron donor [94]. And Chathuranga et al. reported rhodindolizine dye as the first xanthene-based NIR-II dye [95]. Given the considerable library of NIR-I dyes available, the derivatives exhibited enhanced optical properties in the NIR-II window can also be made by engineering NIR-I dyes.

2.2. NIR-II photoacoustic probes

PA imaging combines the merits of optical excitation and acoustic wave detection, leading to reduced tissue scattering and higher resolution in deep tissues. In the past two decades, PA contrast agents have been researched for the application of imaging of brain [14,16,96], blood vessel [15,50], tumor [13,52,97,98], intestine [20,99], bladder [27] and others [19,21,25]. However, unlike the imaging modality of computed tomography or positron emission computed tomography, photoacoustic imaging is limited by penetration depth. The majority of PA imaging contrast agents focused on the NIR-I region. In recent years, NIR-II PA probes, especially organic NIR-II PA probes have advanced rapidly, achieving deeper penetration depth. The key considerations for the design of NIR-II PA probes include longer wavelength in the NIR-II spectral window, high absorption coefficient and light-to-heat conversion extinction coefficient [100], better physical and chemical stability and favorable biosafety [61]. NIR-II PA probes are discussed below with an emphasis of polymer- or small molecule NIR-II dyes. Other NIR-II PA dyes for photoacoustic imaging include polypyrrole nanosheets [101], mesoionic organic molecules [102] et al., but they have not been widely studied.

2.2.1. Semiconducting polymers

Structurally, semiconducting polymers (SPs) used as NIR-II PA probes have a large π-conjugated backbone consisting of alternating electron-rich donor units (D) and electron-deficient acceptor units (A). It is essential to engineer and choose appropriate donor units and acceptor units to mediate optical and physical properties. Also, narrow band gap and bathochromic shift absorption peak to NIR-II spectral window are also desirable for the design and selection of electron-deficient acceptor units. Enabling semiconducting polymers as NIR-II PA probes also need to exhibit large extinction coefficient and high photothermal conversion efficiency. We summary some common strong electron-withdrawing acceptor groups and electron-donating donor groups for the design of SPs as NIR-II PA contrast agents below. Acceptor units include diketopyrrolopyrrole (DPP), benzobisthiadiazole (BBTD), thiadiazoloquinoxaline (TQ), thiadiazolobenzotriazole (TBZ), thienoisoindigo (TII), bezodipyrrolidone and their derivatives, whereas common donor units include thiophene (T), thienothiophene (TT), bithiophene (BT), fluorene (F), benzodithiophene (BDT) and their derivatives. Some representative reported NIR-II semiconducting polymers are summarized in Fig. 6.

The D-A structure is one of the most common structures of NIR-II semiconducting polymers. For example, Jiang et al. designed and synthesized a series of metabolizable NIR-II absorbing semiconducting polymer. They selected strong electron withdrawing unit BBTD as the acceptor (thiophene substituted BBTD are liable to oxidation for biodegradation) while three different donor units including BDT, 2,6-bis (trimethyltin)− 4,8-didodecylbenzo[1,2-b;4,5-b′]dithiophene, and TT were chosen to form three different SPs including PBBT-OT, PBBT-PT, PBBT-DT, respectively. The three SPs achieved strong absorption in the NIR-II region. PBBT-OT and PBBT-PT exhibited similar absorption spectrum at 900–1200 nm, while PBBT-DT displayed broader absorption spectral extending over 1500 nm (Fig. 7**a**). This phenomenon confirmed the importance of receptor selection that would affect the absorption spectrum shift. The encapsulation in amphiphilic copolymer matrix PLGA-PEG, endowed good water solubility of SPs. The resulting SP nanoparticles (termed as SPN-OT, SPN-PT, SPN-DT) had peak absorption at about 1079 nm (Fig. 7**b**). The photothermal conversion efficiency (PCE) measurement indicated that SPN-PT displayed the highest PCE of 53%, followed by 49% for SPN-DT and 36% for SPN-OT, respectively. Also, these SPNs exhibited excellent photostability and biodegradability [46].

D-A1-D-A2 is another common structure of NIR-II SP. The introduction of a second donor unit further increases the conjugated chain length and induces intermolecular charge transfer, resulting in reduction of the band gap and redshift absorption to the NIR-II region. This

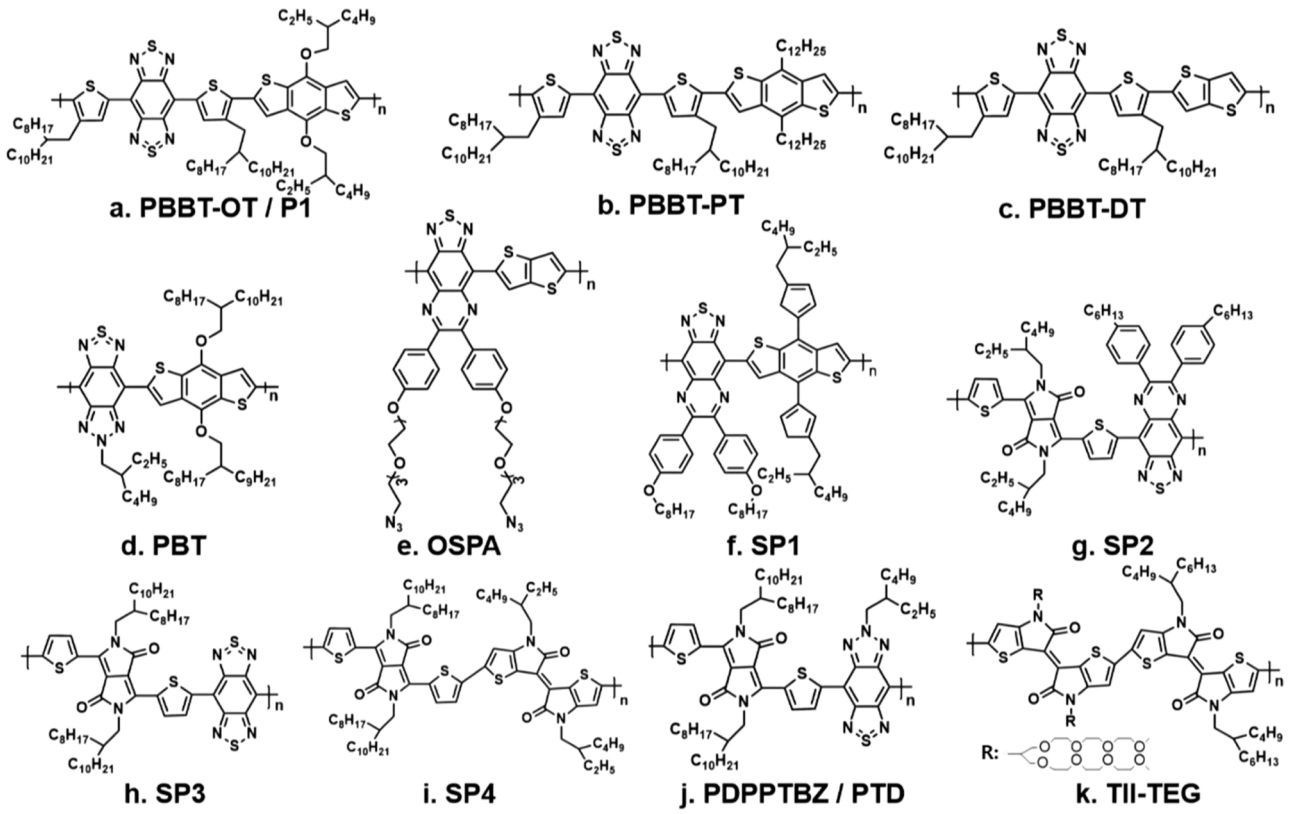

Fig. 6. Typical chemical structure of semiconducting polymers with (a-f): D-A structure; (g-j): D-A1-D-A2 structure; and (k): others.

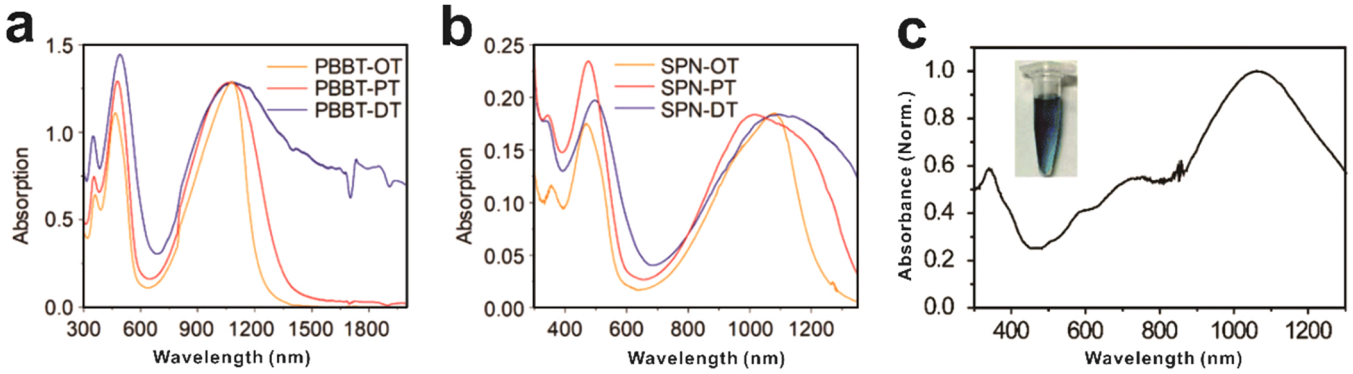

Fig. 7. Absorbance spectra of D-A and D-A1-D-A2 types of NIR-II dyes. a) Absorption spectra of PBBT-OT, PBBT-PT, and PBBT-DT in tetrahydrofuran; b) SPN-OT, SPN-PT, and SPN-DT in PBS buffer [46]. c) Absorption spectrum of PDPPTBZ NPs in water. Inset: photograph of PDPPTBZ NPs (70 μg mL^{-1}) aqueous solution [97]. KGaA, Weinheim, Copyright 2019.
(a) a-b) Reproduced from ref. (b) c) Reproduced from ref. (c) [46] with permission from WILEY-VCH Verlag GmbH & Co. (d) [97] with permission from the Royal Society of Chemistry, Copyright 2019.

expands the library of semiconducting polymers as NIR-II PA probes. Yang et al. developed a typical D-A1-D-A2 structured semiconducting polymer, denoted as PDPPTBZ, with electron-rich thiophene as the donor unit (D) and electron-deficient DPP as the first acceptor unit (A1), and TBZ as the second acceptor. After encapsulation into DSPE-PEG2000 nanoparticles termed PDPPTBZ via nanoprecipitation, PDPPTBZ displayed a broad absorption spectrum ranging from 300 to 1400 nm with the peak around 1064 nm (Fig. 7**c**). The mass extinction coefficient of this NPs reached 43 mg/mLcm^{-1} at the absorption peak. The photothermal conversion efficiency were reported to be as high as 67%. PDPPTBZ also had good colloidal stability and photostability [97].

In addition to D-A and D-A1-D-A2 structures, other conjugated polymers exist that can used for PA contrast agents, such as A-A, A-D-A, or D-D-A-D-D structures, as well as others. However, only a few of these structures are available for NIR-II PA contrast agents. Wu et al. reported an A-A structured conjugated polymer containing TII as electron-deficient unit and this polymer still had absorption in the NIR-II window [103].

2.2.2. *Phthalocyanines*

Phthalocyanines (Pcs) are hydrophobic chromophores with delocalized macrocycle electrons, long absorption wavelengths, and high extinction coefficients that are modulated by chelation of a variety of metals in the center [104,105]. By sophisticated design or modification, Pcs can make NIR-II contrast agents by altering the charge distribution and redshift absorption [20,106]. Zhou et.al used a NIR-II dye

phosphorus Pc (P-Pc) consisting of a central chelated electron-deficient phosphorus element with electron-rich sulfur functionalized benzene in the out layers (Fig. 8a). The absorption peak of P-Pc dissolved in Tween 80 are around 997 nm, while the absorption peak of P-Pc in chloroform reached 1042 nm (Fig. 8b). Importantly, using P-Pc as contrast agents, PA signal was detected through 11.6 cm of chicken breast tissue (under a 1064 nm laser excitation) [20]. Pan et al. developed a cruciform phthalocyanine pentad-based NIR-II dye used as PA probe. Zn_4–H_2[Pc$(OC_{12}H_{17})_{24}$], integrated five monomeric Pc units in its structure with one Pc in the center and four Pcs chelated with the element zinc in the periphery (Fig. 8c). This conjugated framework of Zn_4–H_2[Pc$(OC_{12}H_{17})_{24}$] had absorption peak at 1040 nm and the extinction coefficient could reach up to 5.8×10^5 M^{-1} cm^{-1}. The water soluble Zn_4–H_2Pc/DP NPs made by entrapping Zn_4–H_2[Pc$(OC_{12}H_{17})_{24}$] in DSPE-PEG2000-OCH_3 exhibited a slightly redshifted absorption peak at 1048 nm. And the extinction coefficient was still strong enough and reached to 3.7×10^5 M^{-1} cm^{-1}. Moreover, the Zn_4–H_2Pc/DP NPs had high PCE of 58.3% with excitation by a 1064 nm laser (Fig. 8d) [106].

3. Applications of NIR-II dyes

In contrast to the NIR-I imaging, the advantages of NIR-II imaging include higher resolution and deeper tissue penetration, allowing for improved visualization of anatomical structures and monitoring metabolic process in tissues. As more and more NIR-II dyes have been developed, NIR-II imaging has advanced rapidly. In this section, we discuss applications using NIR-II imaging contrasts such as fluorescence imaging, photoacoustic imaging, multimodal imaging, as well as targeted imaging and activatable imaging.

3.1. Fluorescence imaging

Fluorescence imaging is one of the most convenient and economical imaging modalities. Clinically, it has been used for image-guided surgery with good spatial and temporal resolutions. This noninvasive and nonionizing imaging modality needs relatively low-cost equipment, but has fast response times [107–109]. Du et al. fabricated a NIR-II cyanine dye IR-820 coupled with human serum albumin (HSA) that significantly increased the fluorescence brightness. The resulting IR820-HSA organic complex could be used for the mapping of vascular and lymphatic drainage system as well as the visualization of tumors in vivo. After the IR820-HSA was intravenously injected into C57BL/6 mice, NIR-II fluorescence imaging of the vascular system of the mice was acheived and the right hind limb blood vessels and even small blood vessels in the abdomen area were unambiguously distinguished (Fig. 9a). Next, IR820-HSA was subcutaneously injected in the right footpad of C57BL/6 mice, meanwhile, free IR-820 was injected in the left footpad as a control. It was shown that the lymph vessels and lymph nodes including the popliteal and sciatic ones on the right side exhibited higher fluorescence intensity and clear distribution (Fig. 9b).

It is worth noting that disparate afferent and efferent lymphatic vessels from different positions could also be clearly distinguished (Fig. 9c, d). In addition, the NIR-II fluorescence imaging of tumor was carried out with BALB/c nude mice bearing subcutaneous tumors. The tumors could be clearly delineated after the fluorescence images of mice were recorded at several specific time points post injection of IR820-HSA, (Fig. 9e) [18].

Smart designs and functions of contrast agents have long been the pursuit of researchers in the field. Molecular targeting depends on the binding of targeting ligands to disease-specific receptors that has been widely used to improve contrast agents for disease diagnosis [66,110]. One of the most common strategies for active targeting is directly binding of disease-specific ligands chemically or biologically (for example peptides, proteins, antibodies, etc.) that actively targets receptors over-expressed in disease-related cells [19,65]. Targeted imaging can also increase imaging depth and collect more accurate imaging information using NIR-II dyes. Zhu et al. introduced a target ligand, human chorionic gonadotropin (hCG) to a NIR-II fluorophore IR-FEPC (polyethylene-glycol carboxyl substitutional IR-FE). hCG is a gonadotropin that affects ovarian follicle maturation and effectively target luteinizing hormone (LH) receptor in mouse ovaries. The resulting hCG @IR-FEPC could clearly distinguish three different stages of varies including theca, granulose, and luteal enriched cells. The depth of *ex vivo* 3D fluorescence imaging in mouse ovaries reached 900 μm. In addition, different NIR-II fluorophores with different emissions and targeted ligands could realize multicolor NIR-II imaging of different receptors. Follicle stimulating hormone (FSH) is another gonadotropin that acts in promoting ovarian maturation. Two bioconjugates, hCG@IRFEPC and FSH@lead sulfide (PbS) with fluorescence in the NIR-IIa and NIR-IIb region were also made and successfully achieved in vivo two-color simultaneous imaging of hCG and FSH receptors with considerable imaging depth and resolution in a murine ovary cancer

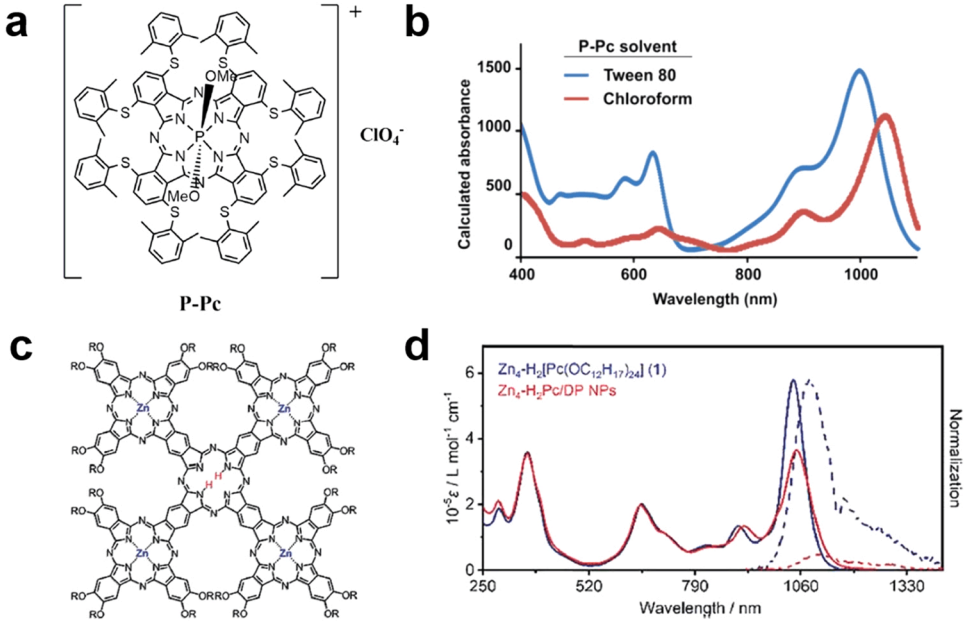

Fig. 8. NIR-II phthalocyanine derivatives and their optical properties. a) Chemical structure of P-Pc. b) Absorbance spectral of P-Pc dye in Tween 80 (blue) and chloroform (red). The mass concentrations were 40 mg/mL and 20 mg/mL, respectively [20]. c) Chemical structure of Zn_4–H_2[Pc$(OC_{12}H_{17})_{24}$]. d) Absorption and fluorescence emission spectra (880 nm laser excitation) of Zn_4–H_2[Pc$(OC_{12}H_{17})_{24}$] in CH2Cl2 and Zn_4–H_2Pc/DP NPs in water [106].
(a) a-b) Reproduced from ref. (b) c-d) Reproduced from ref. (c) [20] with permission from Ivyspring International Publisher, Copyright 2019. (d) [106] with permission from the Royal Society of Chemistry, Copyright 2019.

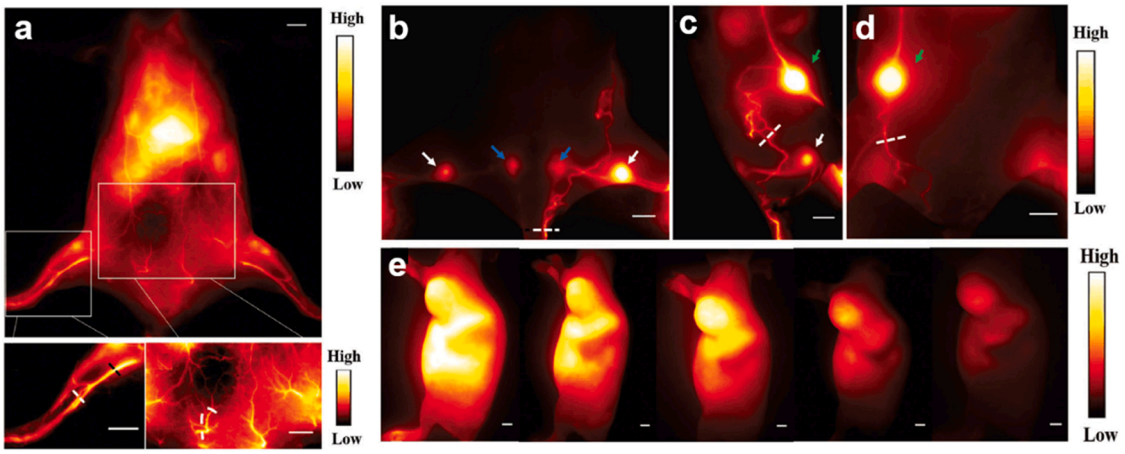

Fig. 9. The application of IR820-HAS used for NIR-II fluorescence imaging. a) NIR-II fluorescence images of the vasculature at 30 min after intravenous administration of IR820–HSA into C57BL/6 mice (imaging details: 1150 LP, 3000 ms). b-d) NIR-II fluorescence image of Popliteal lymph nodes (white arrowheads), sciatic lymph nodes (blue arrowheads) and connected lymphatic vessels, right inguinal lymph node (green arrowheads) and afferent and efferent lymphatic vessels post injection of IR820–HSA (imaging details: 1000 LP, 1000 ms). e) NIR-II fluorescence images of 143B osteosarcoma tumor-bearing mice at a series of specific time points after IR820–HSA injection (imaging details: 1000 LP, 300 ms) [18]. KGaA, Weinheim, Copyright 2019.
(a) Reproduced from ref. (b) [18] with permission from WILEY-VCH Verlag GmbH & Co.

model [19].

3.2. Photoacoustic imaging

Photoacoustic (PA) imaging takes advantage of the optical contrast of endogenous biological molecules or exogenous PA imaging agents. The photoacoustic effect results from the absorption of photons by biological molecules thermoelastically, which generates high pressure around contrast agents and propagates as ultrasonic waves. PA imaging integrates optical excitation with ultrasonic detection that suffers less light scattering but has high contrast and spatial resolution. Therefore, it can achieve deeper tissue imaging up to several centimeter-scale imaging depth in living bodies [111,112]. Compared to fluorescence imaging, PA imaging has the merits of higher spatial resolution and deeper penetration depth and 3-dimentional imaging, although the instrument of PA imaging is generally more expensive and harder to operate,

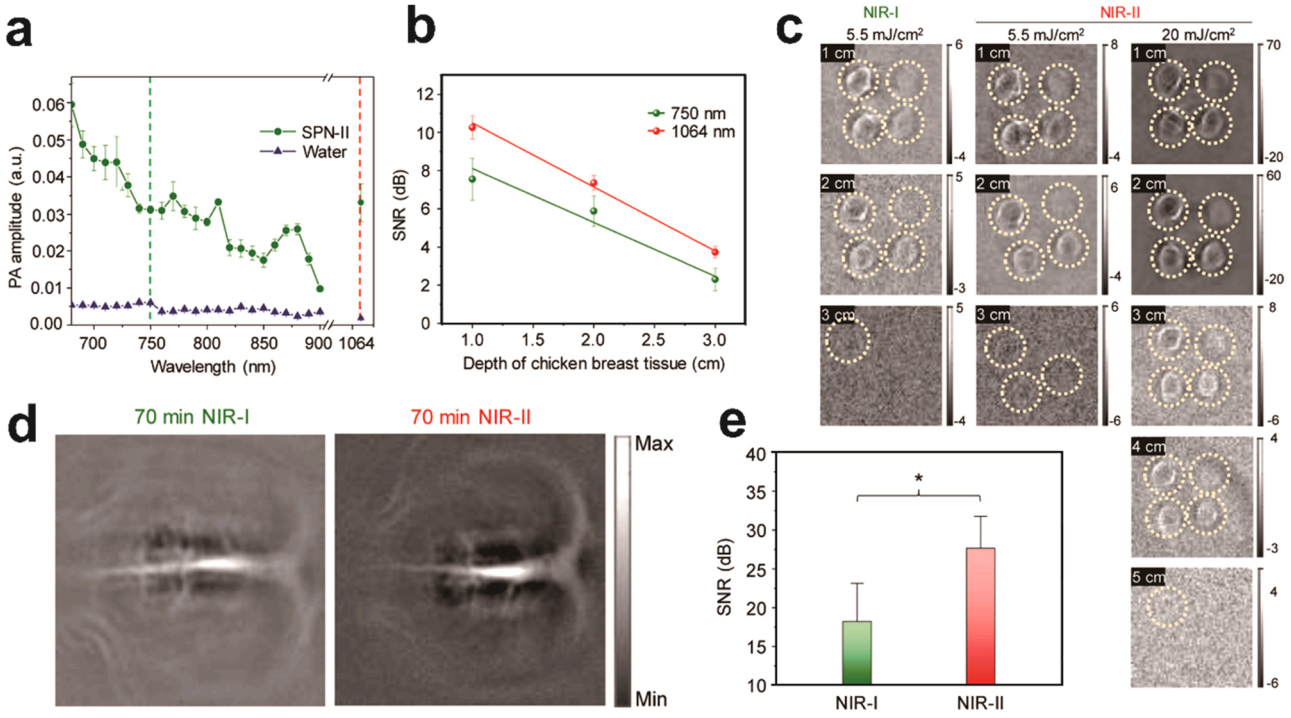

Fig. 10. The application of SPN-II for NIR-II PA imaging. a) PA spectra of SPN-II (200 μg/mL) and water. b) When the mass concentration of SPN-II is 1 mg/mL, SNR change curve with chicken breast tissue depth at 750 and 1064 nm laser, respectively. (Energy density: 5.5 mJ/cm^2. R2 = 0.92549 for 750 nm and 0.99172 for 1064 nm). c) NIR-I and NIR-II PA images of four different concentrations of SPN-II solutions (0.05, 0.2, 0.5, 1 mg/mL) encapsulated by agar gel at different depth. (750 nm laser for NIR-I with 5.5 mJ/cm^2 energy density (left); 1064 nm laser for NIR-II with 5.5 mJ/cm^2 (middle) and 20 mJ/cm^2 (right), respectively). d) Comparison of NIR-I and NIR-II PA images of rat brain at 70 min after SPN-II (1.8 mg/rat) administration via tail vein. e) Comparison of SNR of brain cortex in NIR-I and NIR-II window corresponding to figure e. (750 nm laser for NIR-I and 1064 nm for NIR-II with energy density of 5.5 mJ/cm^2) [50].
(a) Reproduced from ref. (b) [50] with permission from American Chemical Society, Copyright 2017.

limiting its widespread use as fluorescence imaging. There are still many problems to be solved for the translation of PA, such as deeper penetration depth and targeted imaging with high specificity and biosafety of contrast agents. In addition, to improve the PA imaging quality, the use of contrast agents is typically necessary, and the development of more novel and smart photoacoustic probes has played a great role in boosting photoacoustic imaging technology. In particular, PA imaging in the NIR-II window is attracting increasing attention since it can result in improved imaging quality. NIR-II PA imaging becomes a promising diagnostic technique to evaluate various diseases and related physiological and pathological processes, holding great potential for clinical translation [113–116].

Jiang et al. synthesized semiconducting conjugated polymer nanoparticle denoted as SPN-II with both NIR-I and NIR-II light absorption. The PA amplitude of SPN-II at 750 nm and 1064 nm were basically identical (Fig. 10a), which was conducive to intuitive comparison of NIR-I and NIR-II PA imaging to emphasize the advantages of NIR-II imaging. A deliberately designed D-A1-D-A2 type of semiconducting polymer SP2 could be encapsulated in an amphiphilic copolymer (PEG-b-PPG-b-PEG) based nanoparticle with good water-solubility. SPN-IIs with four different concentrations for in vitro deep tissue PA imaging at both 750 nm and 1064 nm were investigated. As shown in Fig. 10c, acquired PA imaging displayed detectable PA signal at two wavelengths under the highest concentration (1 mg/mL), and SNR in the NIR-II region is obviously higher than that in the NIR-I region for all the depths (Fig. 10b). Because laser with longer wavelength allows higher maximum permissible exposure, 1064 nm laser energy density was increased to 20 mJ/cm^2. And imaging depth of 4 and 5 cm was realized for the lowest (0.05 mg/mL) and highest concentration (1 mg/mL), respectively. Furthermore, PA imaging of brain cortex of living rats in both NIR-I and NIR-II window was conducted. Compared to the 750 nm laser, more clear vascular distribution and higher SBR were obtained under 1064 nm (Fig. 10d, e). These results all highlighted the advantages of PA imaging application in the NIR-II region compared to that in the NIR-I region [50].

Recently, Guo and co-workers reported another D-A1-D-A2 structural NIR-II PA contrast agent (PTD NPs) for PA microscopic imaging of ear vasculatures of healthy or angiogenic tumor-bearing mice. PA imaging of ear vasculatures of healthy nude mouse under 1064 nm laser was first studied. Before intravenous injection, obviously no PA signal was observed (Fig. 11a), but the intricate blood vessels even capillary-level microvessels were clearly delineated 5 min after injection of PTD NPs (Fig. 11b). Furthermore, vivid 3D volumetric images were constructed by collecting PA signals in a layer-by-layer fashion (Fig. 11c). Subsequently, mapping of tumor and supervision of tumor angiogenesis were achieved using PTD NPs. As shown in Fig. 11d, e, PA imaging of ears of HepG2 tumor-bearing mice before and after administration of PTD NPs were compared. Finally, 3D images (Fig. 11f) were reconstructed, which is consistent with the results in Fig. 11e. It is obvious that the ear of tumor-bearing mouse had more dense and distorted vasculatures than that of healthy mouse [15]. It was demonstrated that NIR-II PA imaging in the NIR-II region could be used to accurately monitor physiological and pathological processes with higher imaging depth and SBR ratio.

Activatable photoacoustic imaging probes play an important role in early diagnosis of disease [117,118]. Unlike conventional “always on” contrast agents, activatable probes could be specifically activated from initially “off” state to the state of emitting imaging signal in response to some biomarkers or interested molecular events. And the intensity of the emitted signal changes with the concentration of biomarkers. Thus, desirable activatable contrast agents should possess high specificity and high SBR and permit qualitative analysis [119,120]. To date, several

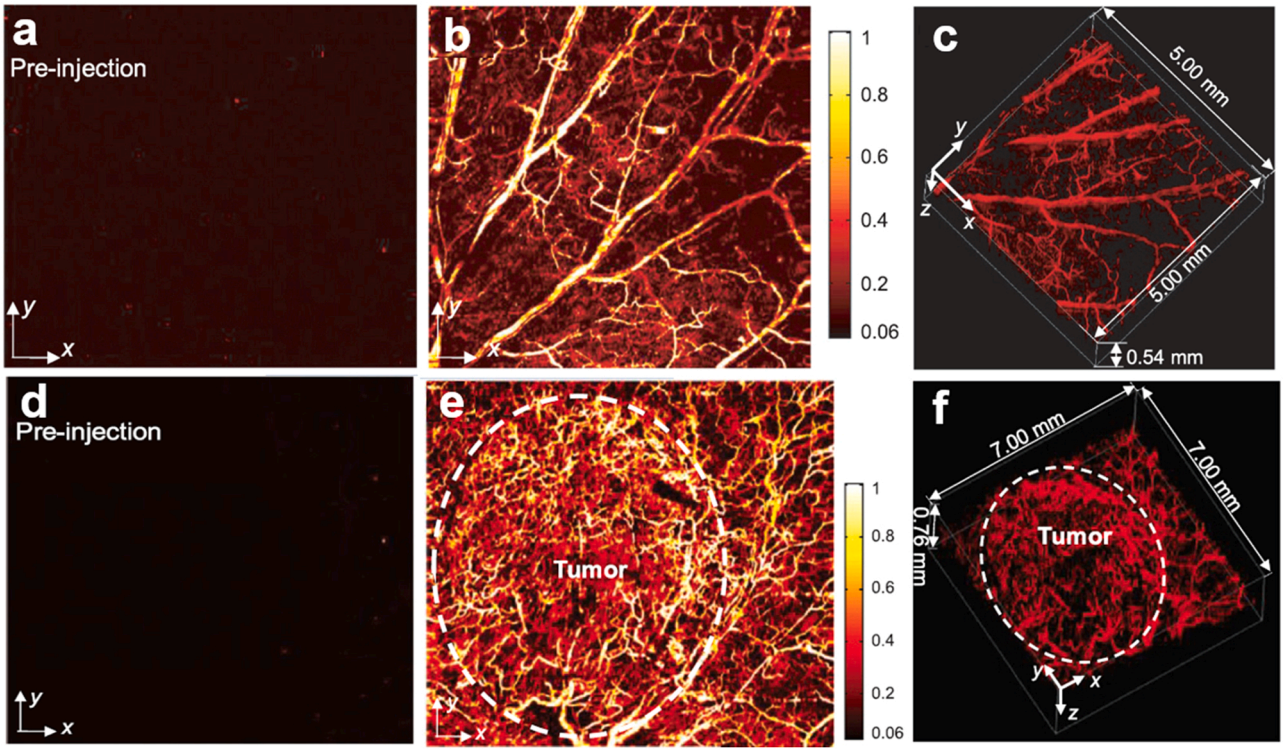

Fig. 11. The application of PTD NPs for NIR-II PA imaging. a, b) Representative two-dimensional ear vasculature imaging of healthy mouse ear (5.00 mm × 5.00 mm, x × y) before (a) and after (b) intravenous injection of PTD NPs. c) 3D ear vasculature image of healthy mouse (5.00 mm × 5.00 mm × 0.54 mm, x × y × z). d, e) Representative two-dimensional imaging of ear of tumor-bearing mouse (7.00 mm × 7.00 mm, x × y) before (d) and after (e) PTD NP injection. f) 3D image ear vasculature of tumor-bearing mouse (7.00 mm × 7.00 mm × 0.76 mm, x × y × z) and white-dashed circle delineated the edges of tumor [15]. KGaA, Weinheim, Copyright 2019.
(a) Reproduced from ref. (b) [15] with permission from WILEY-VCH Verlag GmbH & Co.

activatable probes have been deliberately designed that are suitable for NIR-II imaging to monitor certain pathological conditions, such as tumor hypoxic condition, low pH, reactive oxygen species (ROS), reactive oxygen nitrogen species (RONs) and small molecule mediators.

There are many differences between tumors and normal tissues, one of which is hypoxic environment [69]. Meng et al. designed a hypoxia-triggered probe IR-1048-MZ by conjugating a NIR-II fluorophore (IR-1048) with a nitro imidazole group (2-(2-nitroimidazolyl) ethylamine, MZ). IR-1048-MZ exhibited quenched fluorescence and reduced absorbance due to the electron-withdrawing MZ group. Nitroreductase (NTR), overexpressed in the hypoxia environment, could reduce the MZ group to the amine group, thereby, restoring the NIR-II FL and PA imaging capabilities. As such, the signal intensity related to the level of NTR expression can be used for the evaluation of the degree of hypoxia [77].

RONs including hydroxyl radicals (·OH), hydrogen peroxide (H2O2), peroxynitrite (ONOO-) are important biomarkers in many physiological and pathological processes [121]. For example, the reactive nitrogen species (RNS) ONOO- is considered a representative marker for monitoring early drug-induced hepatotoxicity. Thus, Li et al. developed an activatable NIR-II fluorescent probe IRBTP-B specifically responding to ONOO- by introducing a phenyl borate group into benzothiopyrylium cyanines skeleton. The incorporation of phenyl borate quenched the NIR-II FL emission of IRBTP-B, but once ONOO- removed the masking group phenyl borate, the NIR-II fluorescence signals was activated in response to ONOO-. In the presence of ONOO-, the activated signal of IRBTP-B under up to 5 mm tissue phantom could be detectable. On the contrary, commercially available NIR-I ONOO- probe, D632 can only penetrate 2 mm Intralipid.

Targeted imaging can also assist early detection of diseases. Chen et al. conjugated semiconducting polymer conjugated with tocilizumab (TCZ) and the resulting TCN-PNPs nanoplatform successfully achieved PA diagnosis of early arthritis and imaging-guided treatment [25]. Clearer and enhanced tumor imaging is one of the most important goals of targeted imaging. Guo et al. encapsulated conjugated polymer P1 into NPs by the carrier of DSPE-PEG2000-MAL, then c-RGD peptide, an active targeting ligand for $\alpha_V\beta_3$ integrin receptors on tumor cell surface, was covalently conjugated on the surface of the P1 NPs. The RGD decoration increased the uptake of NP in the tumor and thereby improved imaging quality. To demonstrate the targeting ability of RGD, the comparison of P1GRD NPs and P1 NPs was made for both subcutaneous and brain tumor model, as shown in Fig. 12. After intravenous injection of each NP, the distribution of NPs and resulting changes in PA signal around the tumor area were imaged. For subcutaneous tumor model, it could be clearly seen that the PA signal of the P1RGD NPs group was significantly higher than that of the P1 NPs group at all selected time points (Fig. 12a). And for brain tumor model, both groups displayed PA signals in tumor at 24 h post injection (Fig. 12b). The SBR of the P1RGD NPs group was up to 90 and distinctly higher than that of P1 NPs group (SBR=61) [14]. Compared with the EPR effect alone in the P1 NPs group, the receptor-mediated uptake of P1RGD in tumor cells has obvious advantages in tumor imaging.

The development of emerging contrast agents enables bioimaging of biological tissues from the NIR-I window [122–125] to the NIR-II window [126]. Since the NIR-II dyes has greater penetration depth, the booming development of NIR-II dyes offers more possibilities of imaging of more organs, such as intestinal imaging [91], lymphatic vessel imaging [18], and ovarian cancer imaging [127] in the NIR-II window.

3.3. *Multimodal imaging*

Despite significant improvements using NIR-II dyes, the information available might be limited by just relying on one single imaging modality. NIR-II dye based multimodal imaging with combined desirable features of different imaging modalities could compensate limitations of each single modality, thus providing accurate diagnosis [29,91,93,128].

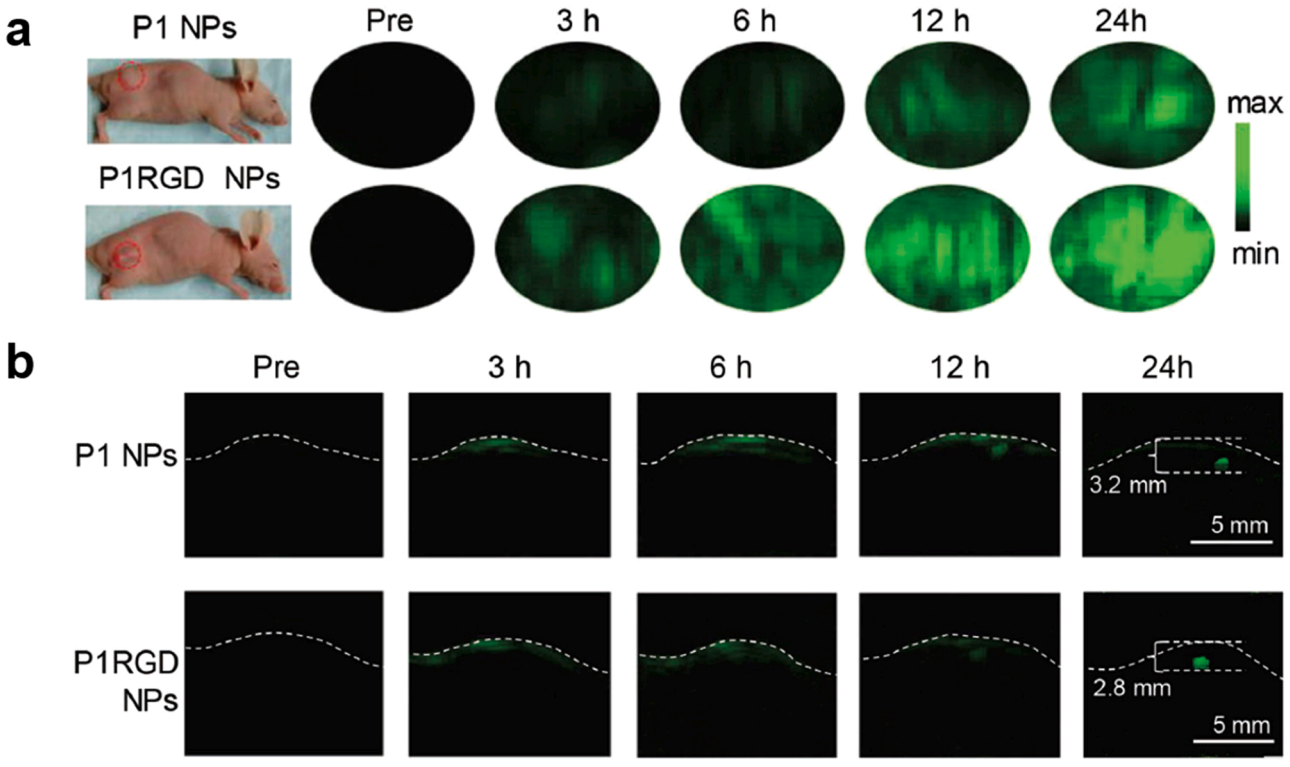

Fig. 12. Comparison of PA imaging of P1 NPs and P1RGD NPs. A series of in vivo PA images of mice bearing subcutaneous U87 xenograft tumor a) and mouse bearing orthotopic brain tumor b) at several selected time points (3, 6, 12, 24 h) following the injection of P1 NPs and P1RGD NPs, respectively. (Imaging details: injection dose = 0.05 mg kg^{-1}, laser wavelength: 1064 nm, laser power: 15 mJ.) [14]. KGaA, Weinheim, Copyright 2018.
(a) Reproduced from ref. (b) [14] with permission from WILEY-VCH Verlag GmbH & Co.

Therefore, it is of potential utility to develop multimodal imaging systems based on NIR-II dyes, especially for the multi-modal nanosystems that can avoid redundant administration and monitoring processes.

FL and PA imaging are amongst the most common dual-mode imaging modalities seen in optical imaging. Some organic NIR-II dyes with absorbance in NIR-I window and fluorescence emission in NIR-II window can provide both NIR-I PA imaging and NIR-II FL imaging. For example, Wang et al. reported an A-D-A structural semiconducting polymer termed DPP-BDT by utilizing DPP and BDT as electron acceptor and donor, respectively [92]. This combines the advantages of fluorescence imaging with high sensitivity and the advantages of PA with high spatial resolution and deep tissue penetration. Furthermore, to obtain more anatomical information, Hu et al. designed a multifunctional semiconducting polymer nanoparticle, PFTQ-PEG-Gd NPs that could achieve tri-modal imaging. In this system, D-A structural semiconducting conjugate were used as PA/NIR-II FL contrast agent, and PFTQ with TQ and fluorene (F) were selected as acceptor and donor. Meanwhile chelated gadolinium ion can be used as a contrast agent of MRI. After systemic injection of PFTQ-PEG-Gd NPs, significantly enhanced PA signal was present within the tumor area in a 4T1 neoplastic mouse over time and reached a plateau value 24 h post-injection. Moreover, the blood vessels connecting the tumor were clearly observed owing to the high resolution of PA imaging (Fig. 13a). Like PA imaging, magnetic signals in the tumor region showed similar trend that the signal intensity gradually increased until 24 h so that anatomical information could be collected (Fig. 13b). Whole-body NIR-II fluorescence images of 4T1 tumorous mice at several time points were obtained after administration of PFTQ-PEG-Gd NPs (Fig. 13c). The maximum fluorescence signals at the tumor locations also appeared one day after injection and the signals gradually decreased due to metabolic clearance. Furthermore, the blood vessels were easily identified utilizing NIR-II FL imaging 2 min after injection (Fig. 13d). Therefore, well-designed PETQ-PEG-Gds NPs showed promise for accurate diagnosis of diseases using multimodal imaging techniques [62].

Guo et al. constructed an NIR-II dye conjugated polymer PBT formed by alternately connecting electron-deficient acceptors and electron-rich donors through Stille coupling polymerization, resulting in PBT NPs via microfluidics. It was the first organic contrast agent with both fluorescence and absorbance in NIR-II window. Using PBT NPs, deciphering deep cerebral vessels and dynamically monitoring the fast-moving arterial blood flows could be realized with high spatial and temporal resolution. Furthermore, with the aid of focused ultrasound opening blood-brain barrier, in vivo NIR-II PA images of early-stage brain tumors and SBR up to 7.2 through the scalp and skull could be obtained. Late-stage brain tumors could be imaged by employing the permeability and retention (EPR) effect alone of PBT NPs. Collectively, PA imaging and FL imaging in the NIR-II window show great potential of diagnosis of deep tissue diseases [16].

4. Conclusion

In the past several years, we have witnessed the emergence of more NIR-II organic contrast agents including cyanine dyes, D-A-D structural dyes and NIR-II PA probes such as semiconducting polymers and phthalocyanines. Several among these could be promising candidates for future translation to clinical imaging because of their merits such as biocompatibility and stability, and tunable optical and chemical properties. Organic NIR-II dyes have been used for the detection of various biological and pathological processes and the diagnosis of diseases with deeper penetration depth and higher resolution. Also, smart NIR-II probes with multi-modal imaging capabilities, targeting properties or activatable performance have also been investigated.

Despite the rapid development of the NIR-II dyes, there still exists room for improvements. Most of the NIR-II dyes were used for imaging near 1000 nm, and new imaging contrast agents for the NIR-II

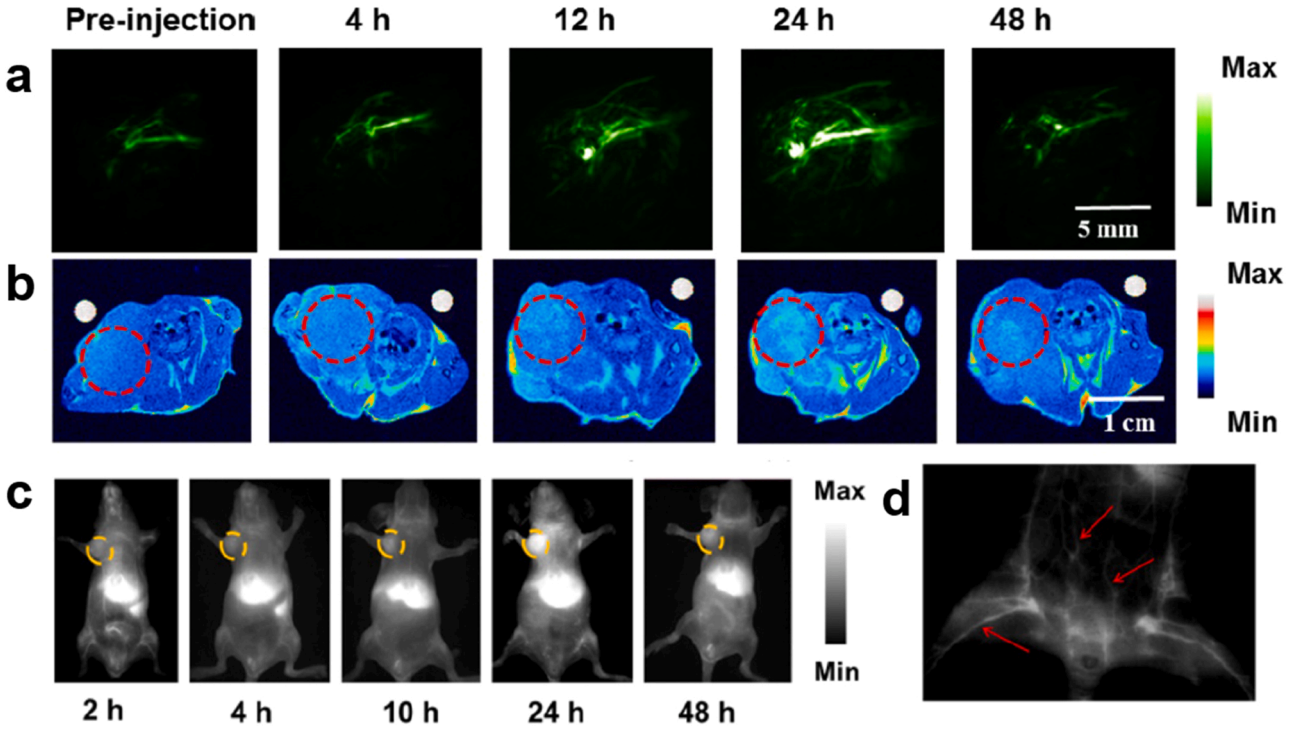

Fig. 13. The application of PFTQ-PEG-Gd NPs for multimodal imaging in the NIR-II region. a) *In vivo* PA imaging, b) MRI, c) NIR-II FL imaging of 4T1 tumorous mouse at indicated time points after intravenous injection of PFTQ-PEG-Gd NPs (150 μL,1 mg/mL). FL imaging was carried out using an 808 nm laser (100 mW cm^{-2}). d) The NIR-II FL imaging of blood vessels (red arrows) of the mouse bearing 4T1 tumor 2 min after PFTQ-PEG-Gd NPs administration under 808 nm excitation [62].
(a) Reproduced from ref. (b) [62] with permission from Ivyspring International Publisher, Copyright 2019.

subwindows such as NIR-IIa and NIR-IIb windows have not been as widely reported. Also, the design of smart NIR-II contrast agents is still in its infancy stage, and more accurate and comprehensive information are usually desired for diagnosis purposes, thereby, developing smart NIR-II contrast agents with high resolution and specificity is highly needed. NIR-II dyes as contrast agents provide a powerful tool for surgeons to identify diseases and delineate anatomical structures. It is expected that with the concerted efforts of chemists, material scientists and eventually physicians, emerging organic smart and enabling NIR-II dyes could add a new chapter to the way diseases can be diagnosed and managed.

Declaration of Competing Interest

The authors have declared that no competing interest exists.

Data Availability

No data was used for the research described in the article.

References

[1] R. Weissleder, Molecular imaging in cancer, Science 312 (2006) 1168–1171, https://doi.org/10.1126/science.1125949.

[2] J.M. Hoffman, S.S. Gambhir, Molecular imaging: the vision and opportunity for radiology in the future, Radiology 244 (2007) 39–47, https://doi.org/10.1148/radiol.2441060773.

[3] A. Fernández, M. Vendrell, Smart fluorescent probes for imaging macrophage activity, Chem. Soc. Rev. 45 (2016) 1182–1196, https://doi.org/10.1039/C5CS00567A.

[4] C. Xie, X. Zhen, Q. Lei, R. Ni, K. Pu, Self-assembly of semiconducting polymer amphiphiles for in vivo photoacoustic imaging, Adv. Funct. Mater. 27 (2017), 1605397, https://doi.org/10.1002/adfm.201605397.

[5] G. Hong, A.L. Antaris, H. Dai, Near-infrared fluorophores for biomedical imaging, Nat. Biomed. Eng. 1 (2017) 0010, https://doi.org/10.1038/s41551-016-0010.

[6] S. Diao, J.L. Blackburn, G. Hong, A.L. Antaris, J. Chang, J.Z. Wu, B. Zhang, K. Cheng, C.J. Kuo, H. Dai, Fluorescence imaging in vivo at wavelengths beyond 1500 nm, Angew. Chem. Int. Ed. 54 (2015) 14758–14762, https://doi.org/10.1002/anie.201507473.

[7] A. Sun, H. Guo, Q. Gan, L. Yang, Q. Liu, L. Xi, Evaluation of visible NIR-I and NIR-II light penetration for photoacoustic imaging in rat organs, Opt. Express 28 (2020) 9002, https://doi.org/10.1364/OE.389714.

[8] Y. Jiang, J. Li, X. Zhen, C. Xie, K. Pu, Dual-peak absorbing semiconducting copolymer nanoparticles for first and second near-infrared window photothermal therapy: a comparative study, Adv. Mater. 30 (2018), 1705980, https://doi.org/10.1002/adma.201705980.

[9] L. Lu, B. Li, S. Ding, Y. Fan, S. Wang, C. Sun, M. Zhao, C.-X. Zhao, F. Zhang, NIR-II bioluminescence for in vivo high contrast imaging and in situ ATP-mediated metastases tracing, Nat. Commun. 11 (2020) 4192, https://doi.org/10.1038/s41467-020-18051-1.

[10] Y. Yang, S. Wang, L. Lu, Q. Zhang, P. Yu, Y. Fan, F. Zhang, NIR-II chemiluminescence molecular sensor for in vivo high-contrast inflammation imaging, Angew. Chem. 132 (2020) 18538–18543, https://doi.org/10.1002/ange.202007649.

[11] K. Shou, Y. Tang, H. Chen, S. Chen, L. Zhang, A. Zhang, Q. Fan, A. Yu, Z. Cheng, Diketopyrrolopyrrole-based semiconducting polymer nanoparticles for in vivo second near-infrared window imaging and image-guided tumor surgery, Chem. Sci. 9 (2018) 3105–3110, https://doi.org/10.1039/C8SC00206A.

[12] H. Wan, H. Ma, S. Zhu, F. Wang, Y. Tian, R. Ma, Q. Yang, Z. Hu, T. Zhu, W. Wang, Z. Ma, M. Zhang, Y. Zhong, H. Sun, Y. Liang, H. Dai, Developing a bright NIR-II fluorophore with fast renal excretion and its application in molecular imaging of immune checkpoint PD-L1, Adv. Funct. Mater. 28 (2018), 1804956, https://doi.org/10.1002/adfm.201804956.

[13] P. Wang, Y. Fan, L. Lu, L. Liu, L. Fan, M. Zhao, Y. Xie, C. Xu, F. Zhang, NIR-II nanoprobes in-vivo assembly to improve image-guided surgery for metastatic ovarian cancer, Nat. Commun. 9 (2018) 2898, https://doi.org/10.1038/s41467-018-05113-8.

[14] B. Guo, Z. Sheng, D. Hu, C. Liu, H. Zheng, B. Liu, Through scalp and Skull NIR-II photothermal therapy of deep orthotopic brain tumors with precise photoacoustic imaging guidance, Adv. Mater. 30 (2018), 1802591, https://doi.org/10.1002/adma.201802591.

[15] B. Guo, J. Chen, N. Chen, E. Middha, S. Xu, Y. Pan, M. Wu, K. Li, C. Liu, B. Liu, High-resolution 3D NIR-II photoacoustic imaging of cerebral and tumor vasculatures using conjugated polymer nanoparticles as contrast agent, Adv. Mater. 31 (2019), 1808355, https://doi.org/10.1002/adma.201808355.

[16] B. Guo, Z. Feng, D. Hu, S. Xu, E. Middha, Y. Pan, C. Liu, H. Zheng, J. Qian, Z. Sheng, B. Liu, Precise deciphering of brain vasculatures and microscopic tumors with dual NIR-II fluorescence and photoacoustic imaging, Adv. Mater. (2019), 1902504, https://doi.org/10.1002/adma.201902504.

[17] Z. Feng, X. Yu, M. Jiang, L. Zhu, Y. Zhang, W. Yang, W. Xi, G. Li, J. Qian, Excretable IR-820 for in vivo NIR-II fluorescence cerebrovascular imaging and photothermal therapy of subcutaneous tumor, Theranostics 9 (2019) 5706–5719, https://doi.org/10.7150/thno.31332.

[18] B. Du, C. Qu, K. Qian, Y. Ren, Y. Li, X. Cui, S. He, Y. Wu, T. Ko, R. Liu, X. Li, Y. Li, Z. Cheng, An IR820 dye–protein complex for second near-infrared window and photoacoustic imaging, Adv. Opt. Mater. 8 (2020), 1901471, https://doi.org/10.1002/adom.201901471.

[19] S. Zhu, S. Herraiz, J. Yue, M. Zhang, H. Wan, Q. Yang, Z. Ma, Y. Wang, J. He, A. L. Antaris, Y. Zhong, S. Diao, Y. Feng, Y. Zhou, K. Yu, G. Hong, Y. Liang, A. J. Hsueh, H. Dai, 3D NIR-II molecular imaging distinguishes targeted organs with high-performance NIR-II bioconjugates, Adv. Mater. 30 (2018), 1705799, https://doi.org/10.1002/adma.201705799.

[20] Y. Zhou, D. Wang, Y. Zhang, U. Chitgupi, J. Geng, Y. Wang, Y. Zhang, T.R. Cook, J. Xia, J.F. Lovell, A phosphorus phthalocyanine formulation with intense absorbance at 1000 nm for deep optical imaging, Theranostics 6 (2016) 688–697, https://doi.org/10.7150/thno.14555.

[21] Y. Lyu, X. Zhen, Y. Miao, K. Pu, Reaction-based semiconducting polymer nanoprobes for photoacoustic imaging of protein sulfenic acids, ACS Nano 11 (2017) 358–367, https://doi.org/10.1021/acsnano.6b05949.

[22] J. Zhang, X. Zhen, P.K. Upputuri, M. Pramanik, P. Chen, K. Pu, Activatable photoacoustic nanoprobes for in vivo ratiometric imaging of peroxynitrite, Adv. Mater. 29 (2017), 1604764, https://doi.org/10.1002/adma.201604764.

[23] S. Wang, Z. Li, Y. Liu, G. Feng, J. Zheng, Z. Yuan, X. Zhang, Activatable photoacoustic and fluorescent probe of nitric oxide for cellular and in vivo imaging, Sens. Actuators B Chem. 267 (2018) 403–411, https://doi.org/10.1016/j.snb.2018.04.052.

[24] D. Li, S. Wang, Z. Lei, C. Sun, A.M. El-Toni, M.S. Alhoshan, Y. Fan, F. Zhang, Peroxynitrite activatable NIR-II fluorescent molecular probe for drug-induced hepatotoxicity monitoring, Anal. Chem. 91 (2019) 4771–4779, https://doi.org/10.1021/acs.analchem.9b00317.

[25] J. Chen, J. Qi, C. Chen, J. Chen, L. Liu, R. Gao, T. Zhang, L. Song, D. Ding, P. Zhang, C. Liu, Tocilizumab–conjugated polymer nanoparticles for NIR-II photoacoustic-imaging-guided therapy of rheumatoid arthritis, Adv. Mater. 32 (2020), 2003399, https://doi.org/10.1002/adma.202003399.

[26] A. Feuchtinger, A. Walch, M. Dobosz, Deep tissue imaging: a review from a preclinical cancer research perspective, Histochem. Cell Biol. 146 (2016) 781–806, https://doi.org/10.1007/s00418-016-1495-7.

[27] B. Park, K.M. Lee, S. Park, M. Yun, H.-J. Choi, J. Kim, C. Lee, H. Kim, C. Kim, Deep tissue photoacoustic imaging of nickel(II) dithiolene-containing polymeric nanoparticles in the second near-infrared window, Theranostics 10 (2020) 2509–2521, https://doi.org/10.7150/thno.39403.

[28] S. Zhu, R. Tian, A.L. Antaris, X. Chen, H. Dai, Near-Infrared-II molecular dyes for cancer imaging and surgery, Adv. Mater. (2019), 1900321, https://doi.org/10.1002/adma.201900321.

[29] S. He, J. Song, J. Qu, Z. Cheng, Crucial breakthrough of second near-infrared biological window fluorophores: design and synthesis toward multimodal imaging and theranostics, Chem. Soc. Rev. 47 (2018) 4258–4278, https://doi.org/10.1039/C8CS00234G.

[30] F. Ding, Y. Zhan, X. Lu, Y. Sun, Recent advances in near-infrared II fluorophores for multifunctional biomedical imaging, Chem. Sci. 9 (2018) 4370–4380, https://doi.org/10.1039/C8SC01153B.

[31] C.F. Chiu, W.A. Saidi, V.E. Kagan, A. Star, Defect-induced near-infrared photoluminescence of single-walled carbon nanotubes treated with polyunsaturated fatty acids, J. Am. Chem. Soc. 139 (2017) 4859–4865, https://doi.org/10.1021/jacs.7b00390.

[32] N.M. Iverson, P.W. Barone, M. Shandell, L.J. Trudel, S. Sen, F. Sen, V. Ivanov, E. Atolia, E. Farias, T.P. McNicholas, N. Reuel, N.M.A. Parry, G.N. Wogan, M. S. Strano, In vivo biosensing via tissue-localizable near-infrared-fluorescent single-walled carbon nanotubes, Nat. Nanotechnol. 8 (2013) 873–880, https://doi.org/10.1038/nnano.2013.222.

[33] A. De La Zerda, C. Zavaleta, S. Keren, S. Vaithilingam, S. Bodapati, Z. Liu, J. Levi, B.R. Smith, T.-J. Ma, O. Oralkan, Z. Cheng, X. Chen, H. Dai, B.T. Khuri-Yakub, S. S. Gambhir, Carbon nanotubes as photoacoustic molecular imaging agents in living mice, Nat. Nanotechnol. 3 (2008) 557–562, https://doi.org/10.1038/nnano.2008.231.

[34] B. Dong, C. Li, G. Chen, Y. Zhang, Y. Zhang, M. Deng, Q. Wang, Facile synthesis of highly photoluminescent Ag 2 Se quantum dots as a new fluorescent probe in the second near-infrared window for in vivo imaging, Chem. Mater. 25 (2013) 2503–2509, https://doi.org/10.1021/cm400812v.

[35] G. Hong, J.T. Robinson, Y. Zhang, S. Diao, A.L. Antaris, Q. Wang, H. Dai, In vivo fluorescence imaging with Ag 2 S quantum dots in the second near-infrared region, Angew. Chem. Int. Ed. 51 (2012) 9818–9821, https://doi.org/10.1002/anie.201206059.

[36] A. Zebibula, N. Alifu, L. Xia, C. Sun, X. Yu, D. Xue, L. Liu, G. Li, J. Qian, Ultrastable and biocompatible NIR-II quantum dots for functional bioimaging, Adv. Funct. Mater. 28 (2018), 1703451, https://doi.org/10.1002/adfm.201703451.

[37] M. Kamimura, T. Matsumoto, S. Suyari, M. Umezawa, K. Soga, Ratiometric near-infrared fluorescence nanothermometry in the OTN-NIR (NIR II/III) biological window based on rare-earth doped β-NaYF 4 nanoparticles, J. Mater. Chem. B 5 (2017) 1917–1925, https://doi.org/10.1039/C7TB00070G.

[38] G. Chen, H. Qiu, P.N. Prasad, X. Chen, Upconversion nanoparticles: design, nanochemistry, and applications in theranostics, Chem. Rev. 114 (2014) 5161–5214, https://doi.org/10.1021/cr400425h.

[39] S. He, S. Chen, D. Li, Y. Wu, X. Zhang, J. Liu, J. Song, L. Liu, J. Qu, Z. Cheng, High affinity to skeleton rare earth doped nanoparticles for near-infrared II imaging,

Nano Lett. 19 (2019) 2985–2992, https://doi.org/10.1021/acs.nanolett.9b00140.
[40] L. Zhang, S. Gao, F. Zhang, K. Yang, Q. Ma, L. Zhu, Activatable hyaluronic acid nanoparticle as a theranostic agent for optical/photoacoustic image-guided photothermal therapy, ACS Nano 8 (2014) 12250–12258, https://doi.org/10.1021/nn506130t.
[41] D. Gao, Z. Sheng, Y. Liu, D. Hu, J. Zhang, X. Zhang, H. Zheng, Z. Yuan, Protein-modified CuS nanotriangles: a potential multimodal nanoplatform for In vivo tumor photoacoustic/magnetic resonance dual-modal imaging, Adv. Healthc. Mater. 6 (2017), 1601094, https://doi.org/10.1002/adhm.201601094.
[42] G. Liu, J. Zhu, H. Guo, A. Sun, P. Chen, L. Xi, W. Huang, X. Song, X. Dong, Mo2C-derived polyoxometalate for NIR-II photoacoustic imaging-guided chemodynamic/photothermal synergistic therapy, Angew. Chem. 131 (2019) 18814–18819, https://doi.org/10.1002/ange.201910815.
[43] X. Cheng, R. Sun, L. Yin, Z. Chai, H. Shi, M. Gao, Light-triggered assembly of gold nanoparticles for photothermal therapy and photoacoustic imaging of tumors in vivo, Adv. Mater. 29 (2017), 1604894, https://doi.org/10.1002/adma.201604894.
[44] J. Zhou, Y. Jiang, S. Hou, P.K. Upputuri, D. Wu, J. Li, P. Wang, X. Zhen, M. Pramanik, K. Pu, H. Duan, Compact plasmonic blackbody for cancer theranosis in the near-infrared II window, ACS Nano 12 (2018) 2643–2651, https://doi.org/10.1021/acsnano.7b08725.
[45] Q. Chen, J. Chen, Z. Yang, L. Zhang, Z. Dong, Z. Liu, NIR-II light activated photodynamic therapy with protein-capped gold nanoclusters, Nano Res 11 (2018) 5657–5669, https://doi.org/10.1007/s12274-017-1917-4.
[46] Y. Jiang, P.K. Upputuri, C. Xie, Z. Zeng, A. Sharma, X. Zhen, J. Li, J. Huang, M. Pramanik, K. Pu, Metabolizable semiconducting polymer nanoparticles for second near-infrared photoacoustic imaging, Adv. Mater. 31 (2019), 1808166, https://doi.org/10.1002/adma.201808166.
[47] P. Cheng, K. Pu, Molecular imaging and disease theranostics with renal-clearable optical agents, Nat. Rev. Mater. 6 (2021) 1095–1113, https://doi.org/10.1038/s41578-021-00328-6.
[48] S. Zhu, B.C. Yung, S. Chandra, G. Niu, A.L. Antaris, X. Chen, Near-Infrared-II (NIR-II) bioimaging via off-peak NIR-I fluorescence emission, Theranostics 8 (2018) 4141–4151, https://doi.org/10.7150/thno.27995.
[49] K. Pu, J. Mei, J.V. Jokerst, G. Hong, A.L. Antaris, N. Chattopadhyay, A. J. Shuhendler, T. Kurosawa, Y. Zhou, S.S. Gambhir, Z. Bao, J. Rao, Diketopyrrolopyrrole-based semiconducting polymer nanoparticles for in vivo photoacoustic imaging, Adv. Mater. 27 (2015) 5184–5190, https://doi.org/10.1002/adma.201502285.
[50] Y. Jiang, P.K. Upputuri, C. Xie, Y. Lyu, L. Zhang, Q. Xiong, M. Pramanik, K. Pu, Broadband absorbing semiconducting polymer nanoparticles for photoacoustic imaging in second near-infrared window, Nano Lett. 17 (2017) 4964–4969, https://doi.org/10.1021/acs.nanolett.7b02106.
[51] F. Ding, C. Li, Y. Xu, J. Li, H. Li, G. Yang, Y. Sun, PEGylation regulates self-assembled small-molecule dye–based probes from single molecule to nanoparticle size for multifunctional NIR-II bioimaging, Adv. Healthc. Mater. 7 (2018), 1800973, https://doi.org/10.1002/adhm.201800973.
[52] C. Yin, X. Li, G. Wen, B. Yang, Y. Zhang, X. Chen, P. Zhao, S. Li, R. Li, L. Wang, C.-S. Lee, L. Bian, Organic semiconducting polymer amphiphile for near-infrared-II light-triggered phototheranostics, Biomaterials 232 (2020), 119684, https://doi.org/10.1016/j.biomaterials.2019.119684.
[53] T. Li, C. Li, Z. Ruan, P. Xu, X. Yang, P. Yuan, Q. Wang, L. Yan, Polypeptide-conjugated second near-infrared organic fluorophore for image-guided photothermal therapy, ACS Nano 13 (2019) 3691–3702, https://doi.org/10.1021/acsnano.9b00452.
[54] W. Zhang, W. Deng, H. Zhang, X. Sun, T. Huang, W. Wang, P. Sun, Q. Fan, W. Huang, Bioorthogonal-targeted 1064 nm excitation theranostic nanoplatform for precise NIR-IIa fluorescence imaging guided efficient NIR-II photothermal therapy, Biomaterials 243 (2020), 119934, https://doi.org/10.1016/j.biomaterials.2020.119934.
[55] Y. Zhu, C. Gu, Y. Miao, B. Yu, Y. Shen, H. Cong, D–A polymers for fluorescence/photoacoustic imaging and characterization of their photothermal properties, J. Mater. Chem. B 7 (2019) 6576–6584, https://doi.org/10.1039/C9TB01196J.
[56] Q. Chen, J. Chen, M. He, Y. Bai, H. Yan, N. Zeng, F. Liu, S. Wen, L. Song, Z. Sheng, C. Liu, C. Fang, Novel small molecular dye-loaded lipid nanoparticles with efficient near-infrared-II absorption for photoacoustic imaging and photothermal therapy of hepatocellular carcinoma, Biomater. Sci. 7 (2019) 3165–3177, https://doi.org/10.1039/C9BM00528E.
[57] G. Wen, X. Li, Y. Zhang, X. Han, X. Xu, C. Liu, K.W.Y. Chan, C.-S. Lee, C. Yin, L. Bian, L. Wang, Effective phototheranostics of brain tumor assisted by near-infrared-II light-responsive semiconducting polymer nanoparticles, ACS Appl. Mater. Interfaces 12 (2020) 33492–33499, https://doi.org/10.1021/acsami.0c08562.
[58] W. Zhang, X. Sun, T. Huang, X. Pan, P. Sun, J. Li, H. Zhang, X. Lu, Q. Fan, W. Huang, 1300 nm absorption two-acceptor semiconducting polymer nanoparticles for NIR-II photoacoustic imaging system guided NIR-II photothermal therapy, Chem. Commun. 55 (2019) 9487–9490, https://doi.org/10.1039/C9CC04196F.
[59] X. Song, X. Lu, B. Sun, H. Zhang, P. Sun, H. Miao, Q. Fan, W. Huang, Conjugated polymer nanoparticles with absorption beyond 1000 nm for NIR-II fluorescence imaging system guided NIR-II photothermal therapy, ACS Appl. Polym. Mater. 2 (2020) 4171–4179, https://doi.org/10.1021/acsapm.0c00637.
[60] J. Li, R. Jiang, Q. Wang, X. Li, X. Hu, Y. Yuan, X. Lu, W. Wang, W. Huang, Q. Fan, Semiconducting polymer nanotheranostics for NIR-II/Photoacoustic imaging-guided photothermal initiated nitric oxide/photothermal therapy, Biomaterials 217 (2019), 119304, https://doi.org/10.1016/j.biomaterials.2019.119304.
[61] J. Mu, M. Xiao, Y. Shi, X. Geng, H. Li, Y. Yin, X. Chen, The chemistry of organic contrast agents in the NIR-II window, Angew. Chem. 134 (2022), https://doi.org/10.1002/ange.202114722.
[62] X. Hu, Y. Tang, Y. Hu, F. Lu, X. Lu, Y. Wang, J. Li, Y. Li, Y. Ji, W. Wang, D. Ye, Q. Fan, W. Huang, Gadolinium-chelated conjugated polymer-based nanotheranostics for photoacoustic/magnetic resonance/NIR-II fluorescence imaging-guided cancer photothermal therapy, Theranostics 9 (2019) 4168–4181, https://doi.org/10.7150/thno.34390.
[63] H. Gong, Z. Dong, Y. Liu, S. Yin, L. Cheng, W. Xi, J. Xiang, K. Liu, Y. Li, Z. Liu, Engineering of multifunctional nano-micelles for combined photothermal and photodynamic therapy under the guidance of multimodal imaging, Adv. Funct. Mater. 24 (2014) 6492–6502, https://doi.org/10.1002/adfm.201401451.
[64] J. Rieffel, F. Chen, J. Kim, G. Chen, W. Shao, S. Shao, U. Chitgupi, R. Hernandez, S.A. Graves, R.J. Nickles, P.N. Prasad, C. Kim, W. Cai, J.F. Lovell, Hexamodal imaging with porphyrin-phospholipid-coated upconversion nanoparticles, Adv. Mater. 27 (2015) 1785–1790, https://doi.org/10.1002/adma.201404739.
[65] X. Xie, Y. Hu, C. Zhang, J. Song, S. Zhuang, Y. Wang, A targeted biocompatible organic nanoprobe for photoacoustic and near-infrared-II fluorescence imaging in living mice, RSC Adv. 9 (2019) 301–306, https://doi.org/10.1039/C8RA08163H.
[66] S. Kurbegovic, K. Juhl, H. Chen, C. Qu, B. Ding, J.M. Leth, K.T. Drzewiecki, A. Kjaer, Z. Cheng, Molecular targeted NIR-II probe for image-guided brain tumor surgery, Bioconjug. Chem. 29 (2018) 3833–3840, https://doi.org/10.1021/acs.bioconjchem.8b00669.
[67] S. Zhu, Q. Yang, A.L. Antaris, J. Yue, Z. Ma, H. Wang, W. Huang, H. Wan, J. Wang, S. Diao, B. Zhang, X. Li, Y. Zhong, K. Yu, G. Hong, J. Luo, Y. Liang, H. Dai, Molecular imaging of biological systems with a clickable dye in the broad 800- to 1,700-nm near-infrared window, Proc. Natl. Acad. Sci. 114 (2017) 962–967, https://doi.org/10.1073/pnas.1617990114.
[68] J. Huang, K. Pu, Activatable molecular probes for second near-infrared fluorescence, chemiluminescence, and photoacoustic imaging, Angew. Chem. 132 (2020) 11813–11827, https://doi.org/10.1002/ange.202001783.
[69] X. Zhang, L. An, Q. Tian, J. Lin, S. Yang, Tumor microenvironment-activated NIR-II reagents for tumor imaging and therapy, J. Mater. Chem. B 8 (2020) 4738–4747, https://doi.org/10.1039/D0TB00030B.
[70] X. Wei, B. Gu (Eds.), Optical Imaging in Human Disease and Biological Research, Springer, Singapore, Singapore, 2021, https://doi.org/10.1007/978-981-15-7627-0.
[71] Z. Zhang, W. Xu, M. Kang, H. Wen, H. Guo, P. Zhang, L. Xi, K. Li, L. Wang, D. Wang, B.Z. Tang, An all-round athlete on the track of phototheranostics: subtly regulating the balance between radiative and nonradiative decays for multimodal imaging-guided synergistic therapy, Adv. Mater. (2020), 2003210, https://doi.org/10.1002/adma.202003210.
[72] T. Ishizawa, N. Fukushima, J. Shibahara, K. Masuda, S. Tamura, T. Aoki, K. Hasegawa, Y. Beck, M. Fukayama, N. Kokudo, Real-time identification of liver cancers by using indocyanine green fluorescent imaging, Cancer 115 (2009) 2491–2504, https://doi.org/10.1002/cncr.24291.
[73] N.S. James, Y. Chen, P. Joshi, T.Y. Ohulchanskyy, M. Ethirajan, M. Henary, L. Strekowsk, R.K. Pandey, Evaluation of polymethine dyes as potential probes for near infrared fluorescence imaging of tumors: part - 1, Theranostics 3 (2013) 692–702, https://doi.org/10.7150/thno.5922.
[74] R. Tian, Q. Zeng, S. Zhu, J. Lau, S. Chandra, R. Ertsey, K.S. Hettie, T. Teraphongphom, Z. Hu, G. Niu, D.O. Kiesewetter, H. Sun, X. Zhang, A. L. Antaris, B.R. Brooks, X. Chen, Albumin-chaperoned cyanine dye yields superbright NIR-II fluorophore with enhanced pharmacokinetics, eaaw0672, Sci. Adv. 5 (2019), https://doi.org/10.1126/sciadv.aaw0672.
[75] R.W. Gao, N. Teraphongphom, E. de Boer, N.S. van den Berg, V. Divi, M. J. Kaplan, N.J. Oberhelman, S.S. Hong, E. Capes, A.D. Colevas, J.M. Warram, E. L. Rosenthal, Safety of panitumumab-IRDye800CW and cetuximab-IRDye800CW for fluorescence-guided surgical navigation in head and neck cancers, Theranostics 8 (2018) 2488–2495, https://doi.org/10.7150/thno.24487.
[76] S. Zhu, Z. Hu, R. Tian, B.C. Yung, Q. Yang, S. Zhao, D.O. Kiesewetter, G. Niu, H. Sun, A.L. Antaris, X. Chen, Repurposing cyanine NIR-I dyes accelerates clinical translation of near-infrared-II (NIR-II) bioimaging, Adv. Mater. 30 (2018), 1802546, https://doi.org/10.1002/adma.201802546.
[77] X. Meng, J. Zhang, Z. Sun, L. Zhou, G. Deng, S. Li, W. Li, P. Gong, L. Cai, Hypoxia-triggered single molecule probe for high-contrast NIR II/PA tumor imaging and robust photothermal therapy, Theranostics 8 (2018) 6025–6034, https://doi.org/10.7150/thno.26607.
[78] B. Li, L. Lu, M. Zhao, Z. Lei, F. Zhang, An efficient 1064 nm NIR-II excitation fluorescent molecular dye for deep-tissue high-resolution dynamic bioimaging, Angew. Chem. 130 (2018) 7605–7609, https://doi.org/10.1002/ange.201801226.
[79] H.I. Kilian, H. Kang, N. Nyayapathi, T. Fukuda, E. Adluru, H. Zhang, B. Quinn, J. Xia, H.S. Choi, J.F. Lovell, Facile formulation of a long-wavelength cyanine for optical imaging in the second near-infrared window, Biomater. Sci. 8 (2020) 4199–4205, https://doi.org/10.1039/D0BM00572J.
[80] Y. Li, H. Zhou, R. Bi, X. Li, M. Zha, Y. Yang, J.-S. Ni, W.H. Liew, M. Olivo, K. Yao, J. Liu, H. Chen, K. Li, Acceptor engineering of small-molecule fluorophores for NIR-II fluorescence and photoacoustic imaging, J. Mater. Chem. B 9 (2021) 9951–9960, https://doi.org/10.1039/D1TB02282B.
[81] G. Qian, J.P. Gao, Z.Y. Wang, Near-infrared chemiluminescence tunable from 900 nm to 1700 nm from narrow-bandgap compounds and polymers, Chem. Commun. 48 (2012) 6426, https://doi.org/10.1039/c2cc32624h.

[82] A.L. Antaris, H. Chen, K. Cheng, Y. Sun, G. Hong, C. Qu, S. Diao, Z. Deng, X. Hu, B. Zhang, X. Zhang, O.K. Yaghi, Z.R. Alamparambil, X. Hong, Z. Cheng, H. Dai, A small-molecule dye for NIR-II imaging, Nat. Mater. 15 (2016) 235–242, https://doi.org/10.1038/nmat4476.
[83] Y. Sun, C. Qu, H. Chen, M. He, C. Tang, K. Shou, S. Hong, M. Yang, Y. Jiang, B. Ding, Y. Xiao, L. Xing, X. Hong, Z. Cheng, Novel benzo-bis(1,2,5-thiadiazole) fluorophores for in vivo NIR-II imaging of cancer, Chem. Sci. 7 (2016) 6203–6207, https://doi.org/10.1039/C6SC01561A.
[84] Y. Sun, M. Ding, X. Zeng, Y. Xiao, H. Wu, H. Zhou, B. Ding, C. Qu, W. Hou, A. Erbu, Y. Zhang, Z. Cheng, X. Hong, Novel bright-emission small-molecule NIR-II fluorophores for in vivo tumor imaging and image-guided surgery, Chem. Sci. 8 (2017) 3489–3493, https://doi.org/10.1039/C7SC00251C.
[85] Q. Yang, Z. Ma, H. Wang, B. Zhou, S. Zhu, Y. Zhong, J. Wang, H. Wan, A. Antaris, R. Ma, X. Zhang, J. Yang, X. Zhang, H. Sun, W. Liu, Y. Liang, H. Dai, Rational Design of Molecular Fluorophores for Biological Imaging in the NIR-II Window, Adv. Mater. 29 (2017), 1605497, https://doi.org/10.1002/adma.201605497.
[86] Q. Yang, Z. Hu, S. Zhu, R. Ma, H. Ma, Z. Ma, H. Wan, T. Zhu, Z. Jiang, W. Liu, L. Jiao, H. Sun, Y. Liang, H. Dai, Donor engineering for NIR-II molecular fluorophores with enhanced fluorescent performance, J. Am. Chem. Soc. 140 (2018) 1715–1724, https://doi.org/10.1021/jacs.7b10334.
[87] Y. Yang, X. Fan, L. Li, Y. Yang, A. Nuernisha, D. Xue, C. He, J. Qian, Q. Hu, H. Chen, J. Liu, W. Huang, Semiconducting polymer nanoparticles as theranostic system for near-infrared-II fluorescence imaging and photothermal therapy under safe laser fluence, ACS Nano 14 (2020) 2509–2521, https://doi.org/10.1021/acsnano.0c00043.
[88] Y. Xu, F. Ren, H. Liu, H. Zhang, Y. Han, Z. Liu, W. Wang, Q. Sun, C. Zhao, Z. Li, Cholesterol-modified black phosphorus nanospheres for the first NIR-II fluorescence bioimaging, ACS Appl. Mater. Interfaces 11 (2019) 21399–21407, https://doi.org/10.1021/acsami.9b05825.
[89] W. Zhang, T. Huang, J. Li, P. Sun, Y. Wang, W. Shi, W. Han, W. Wang, Q. Fan, W. Huang, Facial control intramolecular charge transfer of quinoid conjugated polymers for efficient in vivo NIR-II imaging, ACS Appl. Mater. Interfaces 11 (2019) 16311–16319, https://doi.org/10.1021/acsami.9b02597.
[90] X. Lu, P. Yuan, W. Zhang, Q. Wu, X. Wang, M. Zhao, P. Sun, W. Huang, Q. Fan, A highly water-soluble triblock conjugated polymer for in vivo NIR-II imaging and photothermal therapy of cancer, Polym. Chem. 9 (2018) 3118–3126, https://doi.org/10.1039/C8PY00215K.
[91] X. Lu, J. Chen, J. Li, B. Xia, J. Xu, Q. Wang, C. Xie, Q. Fan, W. Huang, Single nanoparticles as versatile phototheranostics for tri-modal imaging-guided photothermal therapy, Biomater. Sci. 7 (2019) 3609–3613, https://doi.org/10.1039/C9BM00997C.
[92] Q. Wang, B. Xia, J. Xu, X. Niu, J. Cai, Q. Shen, W. Wang, W. Huang, Q. Fan, Biocompatible small organic molecule phototheranostics for NIR-II fluorescence/photoacoustic imaging and simultaneous photodynamic/photothermal combination therapy, Mater. Chem. Front. 3 (2019) 650–655, https://doi.org/10.1039/C9QM00036D.
[93] Q. Wang, Y. Dai, J. Xu, J. Cai, X. Niu, L. Zhang, R. Chen, Q. Shen, W. Huang, Q. Fan, All-in-one phototheranostics: single laser triggers NIR-II fluorescence/photoacoustic imaging guided photothermal/photodynamic/chemo combination therapy, Adv. Funct. Mater. 29 (2019), 1901480, https://doi.org/10.1002/adfm.201901480.
[94] D. Yao, Y. Wang, R. Zou, K. Bian, P. Liu, S. Shen, W. Yang, B. Zhang, D. Wang, Molecular engineered squaraine nanoprobe for NIR-II/photoacoustic imaging and photothermal therapy of metastatic breast cancer, ACS Appl. Mater. Interfaces 12 (2020) 4276–4284, https://doi.org/10.1021/acsami.9b20147.
[95] C.S.L. Rathnamalala, J.N. Gayton, A.L. Dorris, S.A. Autry, W. Meador, N. I. Hammer, J.H. Delcamp, C.N. Scott, Donor–acceptor–donor NIR II emissive rhodindolizine dye synthesized by C–H bond functionalization, J. Org. Chem. 84 (2019) 13186–13193, https://doi.org/10.1021/acs.joc.9b01860.
[96] B. Guo, Z. Sheng, K. Kenry, D. Hu, X. Lin, S. Xu, C. Liu, H. Zheng, B. Liu, Biocompatible conjugated polymer nanoparticles for highly efficient photoacoustic imaging of orthotopic brain tumors in the second near-infrared window, Mater. Horiz. 4 (2017) 1151–1156, https://doi.org/10.1039/C7MH00672A.
[97] Y. Yang, J. Chen, Y. Yang, Z. Xie, L. Song, P. Zhang, C. Liu, J. Liu, A 1064 nm excitable semiconducting polymer nanoparticle for photoacoustic imaging of gliomas, Nanoscale 11 (2019) 7754–7760, https://doi.org/10.1039/C9NR00552H.
[98] C. Yin, G. Wen, C. Liu, B. Yang, S. Lin, J. Huang, P. Zhao, S.H.D. Wong, K. Zhang, X. Chen, G. Li, X. Jiang, J. Huang, K. Pu, L. Wang, L. Bian, Organic semiconducting polymer nanoparticles for photoacoustic labeling and tracking of stem cells in the second near-infrared window, ACS Nano 12 (2018) 12201–12211, https://doi.org/10.1021/acsnano.8b05906.
[99] Y. Zhang, D. Wang, S. Goel, B. Sun, U. Chitgupi, J. Geng, H. Sun, T.E. Barnhart, W. Cai, J. Xia, J.F. Lovell, Surfactant-Stripped Frozen Pheophytin Micelles for Multimodal Gut Imaging, Adv. Mater. 28 (2016) 8524–8530, https://doi.org/10.1002/adma.201602373.
[100] Y. He, Y. Cao, Y. Wang, Progress on photothermal conversion in the second NIR window based on conjugated polymers, Asian J. Org. Chem. 7 (2018) 2201–2212, https://doi.org/10.1002/ajoc.201800450.
[101] X. Wang, Y. Ma, X. Sheng, Y. Wang, H. Xu, Ultrathin polypyrrole nanosheets via space-confined synthesis for efficient photothermal therapy in the second near-infrared window, Nano Lett. 18 (2018) 2217–2225, https://doi.org/10.1021/acs.nanolett.7b04675.
[102] Y. Liu, H. Liu, H. Yan, Y. Liu, J. Zhang, W. Shan, P. Lai, H. Li, L. Ren, Z. Li, L. Nie, Aggregation-induced absorption enhancement for deep near-infrared II photoacoustic imaging of brain gliomas in vivo, Adv. Sci. 6 (2019), 1801615, https://doi.org/10.1002/advs.201801615.
[103] J. Wu, L. You, L. Lan, H.J. Lee, S.T. Chaudhry, R. Li, J.-X. Cheng, J. Mei, Semiconducting polymer nanoparticles for centimeters-deep photoacoustic imaging in the second near-infrared window, Adv. Mater. 29 (2017), 1703403, https://doi.org/10.1002/adma.201703403.
[104] C.J.H. Ho, G. Balasundaram, W. Driessen, R. McLaren, C.L. Wong, U.S. Dinish, A. B.E. Attia, V. Ntziachristos, M. Olivo, Multifunctional photosensitizer-based contrast agents for photoacoustic imaging, Sci. Rep. 4 (2015) 5342, https://doi.org/10.1038/srep05342.
[105] F. Aytan Kiliçarslan, B. Keskin, İ. Erden, A. Erdoğmuş, Synthesis, characterization and electrochemical properties of new phthalocyanines, J. Coord. Chem. 70 (2017) 2671–2683, https://doi.org/10.1080/00958972.2017.1362501.
[106] H. Pan, S. Li, J. Kan, L. Gong, C. Lin, W. Liu, D. Qi, K. Wang, X. Yan, J. Jiang, A cruciform phthalocyanine pentad-based NIR-II photothermal agent for highly efficient tumor ablation, Chem. Sci. 10 (2019) 8246–8252, https://doi.org/10.1039/C9SC02674F.
[107] A.L. Antaris, H. Chen, S. Diao, Z. Ma, Z. Zhang, S. Zhu, J. Wang, A.X. Lozano, Q. Fan, L. Chew, M. Zhu, K. Cheng, X. Hong, H. Dai, Z. Cheng, A high quantum yield molecule-protein complex fluorophore for near-infrared II imaging, Nat. Commun. 8 (2017) 15269, https://doi.org/10.1038/ncomms15269.
[108] X.-D. Zhang, H. Wang, A.L. Antaris, L. Li, S. Diao, R. Ma, A. Nguyen, G. Hong, Z. Ma, J. Wang, S. Zhu, J.M. Castellano, T. Wyss-Coray, Y. Liang, J. Luo, H. Dai, Traumatic brain injury imaging in the second near-infrared window with a molecular fluorophore, Adv. Mater. 28 (2016) 6872–6879, https://doi.org/10.1002/adma.201600706.
[109] Z. Cai, L. Zhu, M. Wang, A.W. Roe, W. Xi, J. Qian, NIR-II fluorescence microscopic imaging of cortical vasculature in non-human primates, Theranostics 10 (2020) 4265–4276, https://doi.org/10.7150/thno.43533.
[110] S. Dharap, Molecular targeting of drug delivery systems to ovarian cancer by BH3 and LHRH peptides, J. Control. Release 91 (2003) 61–73, https://doi.org/10.1016/S0168-3659(03)00209-8.
[111] L. Cui, J. Rao, Semiconducting polymer nanoparticles as photoacoustic molecular imaging probes, WIREs Nanomed. Nanobiotechnol. 9 (2017), https://doi.org/10.1002/wnan.1418.
[112] Y. Jiang, K. Pu, Advanced photoacoustic imaging applications of near-infrared absorbing organic nanoparticles, Small 13 (2017), 1700710, https://doi.org/10.1002/smll.201700710.
[113] Y. Jiang, K. Pu, Molecular fluorescence and photoacoustic imaging in the second near-infrared optical window using organic contrast agents, Adv. Biosyst. 2 (2018), 1700262, https://doi.org/10.1002/adbi.201700262.
[114] K. Huang, Y. Zhang, J. Lin, P. Huang, Nanomaterials for photoacoustic imaging in the second near-infrared window, Biomater. Sci. 7 (2019) 472–479, https://doi.org/10.1039/C8BM00642C.
[115] Q. Chen, W. Qin, W. Qi, L. Xi, Progress of clinical translation of handheld and semi-handheld photoacoustic imaging, Photoacoustics 22 (2021), 100264, https://doi.org/10.1016/j.pacs.2021.100264.
[116] H. Guo, Y. Li, W. Qi, L. Xi, Photoacoustic endoscopy: a progress review, J. Biophoton. 13 (2020), https://doi.org/10.1002/jbio.202000217.
[117] Q. Miao, Y. Lyu, D. Ding, K. Pu, Semiconducting oligomer nanoparticles as an activatable photoacoustic probe with amplified brightness for in vivo imaging of pH, Adv. Mater. 28 (2016) 3662–3668, https://doi.org/10.1002/adma.201505681.
[118] N. Yang, H. Guo, C. Cao, X. Wang, X. Song, W. Wang, D. Yang, L. Xi, X. Mou, X. Dong, Infection microenvironment-activated nanoparticles for NIR-II photoacoustic imaging-guided photothermal/chemodynamic synergistic anti-infective therapy, Biomaterials 275 (2021), 120918, https://doi.org/10.1016/j.biomaterials.2021.120918.
[119] Q. Miao, K. Pu, Emerging designs of activatable photoacoustic probes for molecular imaging, Bioconjug. Chem. 27 (2016) 2808–2823, https://doi.org/10.1021/acs.bioconjchem.6b00641.
[120] Y. Lyu, K. Pu, Recent advances of activatable molecular probes based on semiconducting polymer nanoparticles in sensing and imaging, Adv. Sci. 4 (2017), 1600481, https://doi.org/10.1002/advs.201600481.
[121] X. Zhen, K. Pu, Development of optical nanoprobes for molecular imaging of reactive oxygen and nitrogen species, Nano Res 11 (2018) 5258–5280, https://doi.org/10.1007/s12274-018-2135-4.
[122] Z. Jiang, B. Sun, Y. Wang, H. Gao, H. Ren, H. Zhang, T. Lu, X. Ren, W. Wei, X. Wang, L. Zhang, J. Li, D. Ding, J.F. Lovell, Y. Zhang, Surfactant-stripped micelles with aggregation-induced enhanced emission for bimodal gut imaging in vivo and microbiota tagging ex vivo, Adv. Healthc. Mater. 10 (2021), 2100356, https://doi.org/10.1002/adhm.202100356.
[123] X. Yang, J.F. Lovell, Y. Zhang, Ingestible contrast agents for gastrointestinal imaging, ChemBioChem 20 (2019) 462–473, https://doi.org/10.1002/cbic.201800589.
[124] Y. Zhang, H. Hong, B. Sun, K. Carter, Y. Qin, W. Wei, D. Wang, M. Jeon, J. Geng, R.J. Nickles, G. Chen, P.N. Prasad, C. Kim, J. Xia, W. Cai, J.F. Lovell, Surfactant-stripped naphthalocyanines for multimodal tumor theranostics with upconversion guidance cream, Nanoscale 9 (2017) 3391–3398, https://doi.org/10.1039/C6NR09321C.
[125] Y. Zhang, M. Jeon, L.J. Rich, H. Hong, J. Geng, Y. Zhang, S. Shi, T.E. Barnhart, P. Alexandridis, J.D. Huizinga, M. Seshadri, W. Cai, C. Kim, J.F. Lovell, Non-invasive multimodal functional imaging of the intestine with frozen micellar naphthalocyanines, Nat. Nanotechnol. 9 (2014) 631–638, https://doi.org/10.1038/nnano.2014.130.

[126] Y. Ding, B. Park, J. Ye, X. Wang, G. Liu, X. Yang, Z. Jiang, M. Han, Y. Fan, J. Song, C. Kim, Y. Zhang, Surfactant-stripped semiconducting polymer micelles for tumor theranostics and deep tissue imaging in the NIR-II window, Small 18 (2022), 2104132, https://doi.org/10.1002/smll.202104132.
[127] Z. Wang, X. Sun, T. Huang, J. Song, Y. Wang, A sandwich nanostructure of gold nanoparticle coated reduced graphene oxide for photoacoustic imaging-guided photothermal therapy in the second NIR window, Front. Bioeng. Biotechnol. 8 (2020) 655, https://doi.org/10.3389/fbioe.2020.00655.
[128] J. Rieffel, U. Chitgupi, J.F. Lovell, Recent advances in higher-order, multimodal, biomedical imaging agents, Small 11 (2015) 4445–4461, https://doi.org/10.1002/smll.201500735.

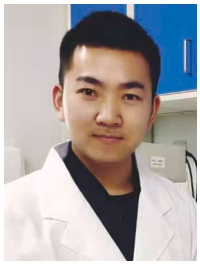

Zhen Jiang is currently a Ph.D. student majoring in school of chemical engineering and technology, Tianjin University. He obtained his master degree at Tianjin university in 2021. His research interests include aggregation-induced emission materials for intestinal imaging.

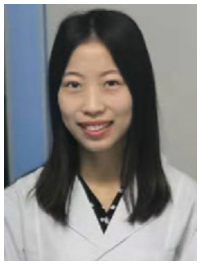

Yuanmeng Ding obtained her undergraduate degree at China University of Petroleum in 2019 and her master degree at Tianjin university in 2022. Her research interest involves developing new contrast agents in the near-infrared II window for theranostics.

Jonathan F Lovell is an Empire Innovation Professor in the Biomedical Engineering Department at University at Buffalo, NY, USA. He received his Ph.D. from University of Toronto. Previously, he completed his MS in Biochemistry at McMaster University in Hamilton, Ontario and his undergraduate degree at the University of Waterloo in Systems Design Engineering.

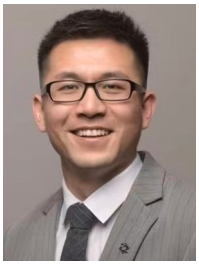

Yumiao Zhang is a professor in the Chemical Engineering Department at Tianjin University, China, since 2018. He obtained his dual bachelor degrees from Nankai University (Chemistry) and Tianjin University (Chemical Engineering) in 2010. And he received his Ph.D. degree (Chemical and Biological Engineering) from University at Buffalo, NY, USA. Then he went to UC Berkeley for his postdoc training. Afterwards, he came back to Tianjin University for his independent research in 2018.